https://doi.org/10.1016/j.coastaleng.2021.104000

Numerical study on impacts of a concurrent storm-tide-tsunami event in Macau and Hong Kong

Jinghua Wang[1,2,5] and Philip L.-F. Liu[1,3,4]

[1]Department of Civil and Environmental Engineering, National University of Singapore, Singapore
[2]Department of Ocean Engineering, Ocean University of China, Qingdao, China
[3]School of Civil and Environmental Engineering, Cornell University, Ithaca, NY, USA
[4]Institute of Hydrological and Ocean Research, National Central University, Taoyuan City, Taiwan
[5]Department of Civil and Environmental Engineering, The Hong Kong Polytechnic University, Hong Kong

Abstract

Intensified activities of tropical cyclones in the Western North Pacific have imposed increasing threats to coastal cities in the context of global climate change. A storm surge superimposed with astronomical high tide, i.e., a storm-tide event, often causes severe flooding in many coastal cities in South China Sea (SCS) region. Meanwhile, the potential tsunami hazard associated with the megathrust in Manila subduction zone has become a serious concern in this region. These two kinds of coastal hazard have been studied independently in the past since they are caused by different physical mechanisms in nature. However, there is no scientific reason to rule out the possibility of concurrence of a storm-tide-tsunami event, which is admittedly rare. This study simulates a group of synthetic events assuming that tsunami waves are generated by a M_w 9 earthquake in the Manila subduction zone during a typhoon, which has the same characteristics as the 2017 Typhoon Hato. A numerical model package originally developed for storm-tide calculation has been modified to simulate a concurrent storm-tide-tsunami event. A variety of scenarios are considered as the tsunamis are superimposed at different phases of the storm-tide event. Their compound impacts on Macau and Hong Kong in Pearl River Delta, China, are investigated. Specifically, the results of water level, arrival time of the maximum water level, flow velocity, and inundation depth are discussed. The worst-case scenarios have been identified at Macau and Hong Kong, respectively. The scenario with tsunami being initiated at 07:00 on 23-Aug-2017 leads to an inundated area of 12.0km^2 in Macau. On the other hand, the scenario with tsunami being started at 08:10 on the same day generates an inundation area of 8.9km^2 in the vicinity of Kai Tak terminal region in Hong Kong. In addition, the efficacy of the linear superposition of results obtained separately for each hazard (i.e., typhoon and tsunamis) is also discussed. Generally speaking, the differences between the linearly superimposed solutions and fully coupled results vary temporally and spatially and could be either positive or negative. However, the linearly superimposed solutions consistently underestimate the maximum water elevation and yield delays on the arrival times of peak flooding stage in the Pearl River estuary. It is concluded that for coastal protection and hazard mitigation planning in this region, these extreme situations need to be considered. A fully coupled numerical model package is now available for conducting such studies.

1 Introduction

Climate change has imposed increasing threats to coastal cities globally. Recent studies have pointed out that the probability of occurrence for tropical cyclones in the Western North Pacific will increase by about 10% in the near future (Chen, et al., 2020). Coastal flooding as a consequence of intensified extreme weather conditions will become a key challenge to many coastal cities in South China Sea (SCS) region. The Pearl River Delta (PRD) is one of the highly populated areas in the SCS region, especially Macau and Hong Kong. These cities have often experienced severe coastal flooding, induced by storm-tide (superposition of high tide and storm surge during a typhoon) events, causing fatalities and economic loss. Another potential coastal geo-hazard in the SCS region is the inundation caused by

tsunamis. It has long been recognized that the Manila subduction zone is a major source for generating mega-tsunamis. Although the historical record on tsunami events is sparse (Li, et al., 2016), the needs for assessing potential tsunami hazards in this region have become increasingly demanding (Sepúlveda, et al., 2019).

These two kinds of coastal geo-hazards and the resultant coastal inundations in Macau and Hong Kong have been studied separately in the past (Li, et al., 2016; Chen, et al., 2019; Sepúlveda, et al., 2019; Yang, et al., 2019; Takagi, et al., 2018). However, the assessment of coastal flooding caused by the concurrence of both geo-hazards in the SCS region has not been performed. It is obvious that the probability of concurrence of any two hazards is lower than that for each hazard. Therefore, the concurrence of a typhoon and a tsunami has conventionally viewed as a rare event and dismissed. However, there is no scientific reason to totally rule out the possibility of such a concurrence in the future. Given the urgent need of assessing future risk of coastal hazards, developing a simulation tool for quantifying the impacts of these natural hazards, separately and concurrently, in the SCS region is the main motivation of this study.

To achieve this goal, a synthetic event in the SCS region is studied in detail herein. Specifically, the 2017 Typhoon Hato is selected as the "future" storm event. The time histories of atmospheric data, including winds and atmospheric pressures, and the tide and wave conditions are assumed to remain the same during the synthetic event. During Typhoon Hato, the combination of high tide and strong storm surge caused widespread coastal flooding in Macau (Li, et al. 2017, Takagi, et al. 2018, Yang, et al. 2019). During the same typhoon the water level in Hong Kong went up by about 1 to 2 metres, and the water level measured at Quarry Bay reached the second highest record since 1954 (HKO, 2017). In the synthetic event, a tsunami is initiated during the future Hato-like typhoon. The tsunami is generated by an earthquake on the northernmost segment of Manila subduction zone with magnitude of $M_W = 9$, which is one of the scenarios studied in Sepulveda, et al. (2019). According to Sepulveda, et al. (2019), the tsunami generated by this earthquake could result in a water level of 3.5m at the Kai Tak cruise terminal in Hong Kong. The severeness of the coastal impact of the synthetic event could vary both spatially and temporally, depending on the timing of the initiation of the tsunami during the typhoon event, which will be investigated in this paper.

To simulate the synthetic event, the two-way coupled SCHISM-WWMIII model package (Zhang & Baptista, 2008; Zhang, et al., 2016) is employed. Recently, SCHISM-WWMIII has been successfully used to hindcast several typhoon events in the SCS region (Shih, et al., 2018; Hsiao, et al., 2020; Hsiao, et al., 2020; Yang, et al., 2021), including the 2017 Typhoon Hato (Yang, et al., 2019). It was also used to simulate tsunamis (Zhang & Baptista, 2008) and study tide-tsunami interactions (Zhang, et al., 2011; Zhang, et al., 2015). In this study, SCHISM-WWMIII is modified slightly to allow the initiation of tsunami during the simulation of a typhoon event. Numerical results are used to examine the impacts of concurrent storm-tide-tsunami hazard in Macau and Hong Kong.

When the generation mechanisms of two hazards are independent of each other, it is often asked if the impact of combined hazards can be obtained by the linear superposition of those from each hazard without considering interactions between them. In this paper, we shall address such a question. To facilitate the discussions the following terminologies and notations are introduced for clarity and brevity. We define the **Composite Model (CM)** as the linear superposition of the results obtained separately from each individual hazard. On the other hand, we define the **Full Model (FM)** as the dynamical coupling of two hazards in one simulation.

The remainder of this paper is structured as follows. Section 2 introduces the geographical features of Macau and Hong Kong, as well as the typhoon characteristics and tsunami conditions for the synthetic event. Section 3 describes the numerical model to be used in the study and its validations. Specifically, the numerical scheme to trigger the tsunami waves in the model is explained. The numerical results and discussions are presented in Section 4. Section 5 concludes the paper.

2 Geographical features, characteristics of typhoon conditions and tsunami source

The Pearl River Delta (PRD) is a funnel-shaped estuary. The width of the estuary mouth is about 50 km with a depth of 40m, and the estuary narrows to 6km wide in the depth of 10m at the head of PRD. Macau city is located on the west side of the estuary and city's south and east coast is exposed to the open ocean. The Inner Harbour is situated on the west coast of the Macau Peninsula in the northern part of the Macau city and is the main transportation hub connecting Macau with adjacent cities in China. This region is connected to the Modaomen Waterway via the Maliuzhou Waterway on the west side of the city. Hong Kong, being located on the eastern coast of the PRD, is a bigger city in terms of size and population, and consists of over 200 islands surrounded by the South China Sea (SCS). Kowloon Bay is located on the southeast side of the Kowloon Peninsula and to the north of Hong Kong Island, and is an important cruise terminal. The bay has a maximum water depth about 40m and is connected with the SCS through a narrow entrance on its east side known as Lei Yue Mun. Figure 1 provides a view of the geographic features around the PRD region, in which the contour lines of the bathymetry in the vicinity of the mouth of PRD are also shown.

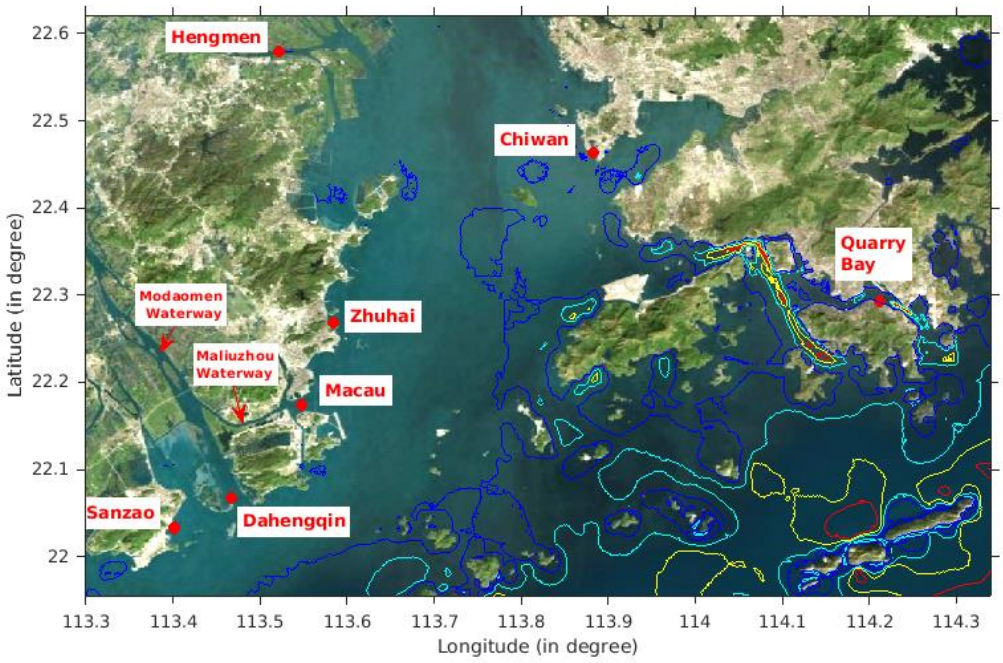

Figure 1. Locations of tidal stations and water depth contour lines in the PRD region. Red: 40m contour; yellow: 30m contour; cyan: 20m contour; blue: 10m contour. Credit is given to Microsoft® Bing Maps®, from which the satellite image is extracted for producing this figure.

2.1 Meteorological conditions of 2017 Typhoon Hato

The PRD region is struck by tropical cyclones (TCs) from May to September annually. Typhoon Hato in 2017 was one of the strongest TCs on the record that made landfall in PRD. Typhoon Hato's formation, propagation, and coastal flooding impacts have been recently investigated by many

researchers (Li, et al., 2018; Chen, et al., 2019; Pun, et al., 2019; Yang, et al., 2019). Considering its severity in terms of coastal flooding, this TC is selected as the "synthetic scenario" for the present study. Here, the meteorological conditions are briefly described for completeness. For more details, readers can refer to the field survey study presented in Li, et al. (2018).

Typhoon Hato originated as a tropical depression in the east of Luzon on 21-Aug-2017. It then moved north-westward reaching the coastal areas of the PRD, where it suddenly intensified and made the landfall in Zhuhai, Guangdong, China, as a Category 3 typhoon (on the Saffir-Simpson scale) at 12:50 UTC+8hr on 23-Aug-2017, as indicated in Figure 2(a). The estimated 10-min maximum sustained wind speed was 165 km/h and the minimum central pressure was 945 hPa (SMG, 2017). It has been pointed out that the intensification of the storm and the concurrent astronomical high tide were the major factors for causing the widespread coastal flooding in Macau (Li, et al., 2018; Yang, et al., 2019), resulting in at least ten deaths and more than 240 injuries. The direct economic loss exceeded 8.3 billion MOP (HKO, 2017). Meanwhile, the storm surge induced by Typhoon Hato raised the water level in Hong Kong by about 1 to 2 metres, and the water level measured at Quarry Bay reached the second highest record since 1954. Many low-lying areas experienced serious flooding during the event leading to the urgent evacuation of residents. Extensive interruption to electricity and transportation was reported (HKO, 2017). Unless mentioned otherwise, the date and time in this study are in local time (UTC+8hr).

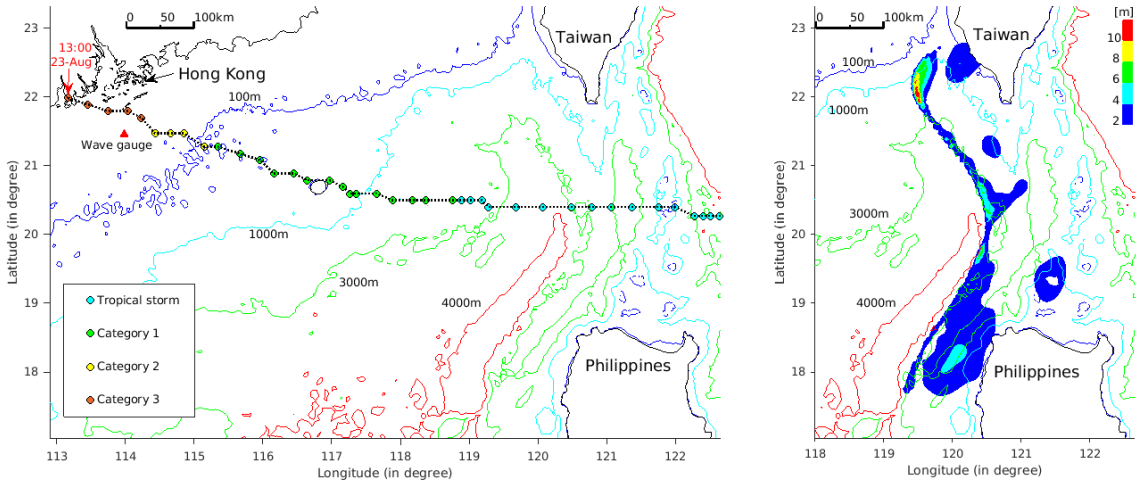

(a) Track of Typhoon Hato (b) Displacement of seafloor

Figure 2. (a) The track of 2017 Typhoon Hato with one-hour interval. The track information is obtained from the China Typhoon Weather website (http://www.weather.com.cn/zt/tqzt/2760639.shtml). Circular dots indicate the locations of typhoon centre. Typhoon Hato made its landfall at 12:50 on 23-Aug-2017. (b) The vertical seafloor displacement (or initial sea surface elevation of the tsunami wave from MSL). In both panels, the contour lines denote the water depth. Red: 4000m; Yellow: 3000m; Cyan: 1000m; Blue: 100m.

2.2 Characteristics of the tsunami

Since the SCS is sheltered by islands and submarine mountain chains, the most hazardous tsunami sources are located within the SCS (Sepúlveda, et al., 2019). In particular, the Manila subduction zone can potentially generate magnitude $M_W > 8.0$ earthquakes and produce extremely devastating tsunamis in SCS (Liu, et al., 2009; Megawati, et al., 2009; Okal, et al., 2011; Terry, et al., 2017). Three fault segments have been identified in the Manila subduction zone (e.g., Li, et al., 2016). Although the

probability of rupturing the entire Manila subduction zone in one single event is extremely low, it cannot be completely ignored (Terry, et al., 2017). However, in the present work, tsunamis generated by the sudden rupture of the northernmost segment with a moment magnitude of $M_W = 9$ are studied. It is one of the scenarios studied in Sepulveda, et al. (2019), which is associated with the largest tsunamis impacting on Hong Kong. For this scenario, the fault plane is 575km long and 191km wide in the strike and dip directions, respectively, where the strike angle is 10^o with the dip angle being 15^o from seafloor to 30 km depth and 30^o in deeper depth. The rake/slip angle is assumed to be 90^o. Using the Okada's linear elastic dislocation theory (Okada, 1985) with the earth crust rigidity being 40GPa, the earthquake induced seafloor deformation can be estimated and is shown in Figure 2 (panel b), where the maximum vertical displacement is over 15m near Taiwan. Such an earthquake event is extremely rare and its return period is estimated to range from ~10^3 to ~10^4 years, depending on the employed reoccurrence model. However, Sepulveda, et al. (2019) showed that there is a 50% probabilty for this $M_W = 9$ earthquake to generate tsunami amplitudes exceeding 3.5m at the Kai Tak cruise terminal, and a 5% probability to cause inundation in vicinity of Hong Kong (Sepúlveda, et al., 2019). Although it has been shown that the tsunami generated by such an earthquake is hazardous to Hong Kong, the impact of the same tsunami to Macau has not been studied. Intuitively speaking, one may expect smaller tsunami waves arriving at Macau, since the distance from the source region to Macau is longer than that to Hong Kong. This is in contrast to the impact of Typhoon Hato, which flooded Macau more severely. Knowing the contrasting consequences in the two cities caused by two independent geo-hazard events renders an interesting opportunity to study the compound impacts. In this study, we use the same Manning's n for tsunami-alone, storm-tide-alone and concurrent storm-tide-tsunami simulations in order to be consistent for making comparisons. More details are provided in section 3.1.

3 Numerical model, configurations, and strategy for tsunami intervention

In this paper the two-way coupled SCHISM-WWMIII model package (Zhang, et al., 2016) will be used to calculate the sea surface levels, the velocity field, and wave field associated with a combination of typhoon and tsunami event. The SCHISM (Semi-implicit Cross-scale Hydroscience Integrated System Model) is a derivative product built from the original SELFE (Semi-implicit Eulerian-Lagrangian Finite-Element) model. The details of the model package can be found in Zhang & Baptista (2008) and Zhang, et al. (2016) and will not be repeated here. The SCHISM is coupled with the third-generation spectral wind wave model, WWMIII (Wind Wave Model III), solving the wave action equation. The details of this wave spectrum model can be found in Roland (2008) and Roland, et al. (2009). The wave spectrum model and SCHISM share the same suite of unstructured mesh. In this study, SCHISM-WWMIII is employed to simulate concurrent storm surge/tide-tsunami event.

3.1 Configurations of the numerical model and validation for Typhoon Hato

As shown in Figure 3, the computational domain covers the SCS region from 105.6^oE to 129.2^oE in Longitude and from 13.6^oN to 28.8^oN in Latitude, and is discretised into ~1 million nodes and ~2 million triangular elements. The grid size gradually decreases from ~50km in the deep sea to ~3km near the Manila trench (earthquake source region), then further reduces to ~1km over the continental shelf and becomes the finest of 20m in the vicinities of Macau and Kowloon Bay area in Hong Kong. The spatial distribution of the nodal points is illustrated in Figure 3. The spectral wave model WWMIII is implemented with 35 wave frequency bins covering the spectral band from 0.039Hz to 1Hz and 24 direction bins with 15° interval. The value of 0.01m is selected as the minimum water depth to determine

whether the shoreline element is dry or wet during the inundation processes. The Manning's n coefficient is assumed to be 0.012 in the area below MSL and 0.025 in the overland area, respectively (Yang, et al., 2019). The water surface elevation and current velocity in SCHISM are updated every 10s and the directional spectra in WWMIII are updated every 600s. The models are two-way coupled and exchange data every 600s. The wave effects on the storm-tide field are through the wave radiation stresses, and storm-tide effects on wave spectra are through time-varying water level and current velocity.

Along the open ocean boundaries (as indicated by the red dashed lines in Figure 3), the re-analysis tide data, based on the FES2014 (Finite Element Solution 2014) tide model (Carrere, et al., 2015), and the hindcast wave data, based on the WAVEWATCH III (available at IFREMER FTP server: ftp.ifremer.fr/ifremer/ww3/HINDCAST/), are employed as the boundary conditions for the coupled model. The latter is also used as the initial condition for the WWMIII model, whereas the SCHISM model starts from the still water level. On the land side of the computational domain, an annually mean runoff of 2,800 m^3/s (Gong & Shen, 2011) is imposed in the Modaomen Waterway.

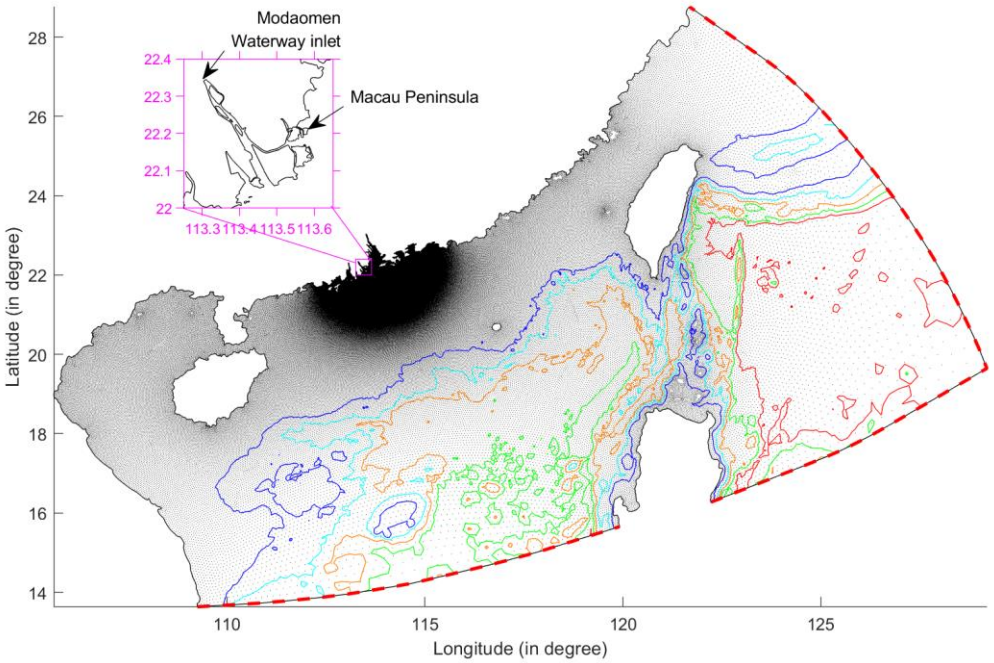

Figure 3. Illustration of the computational domain with bathymetry contours and nodes of triangular elements (black dots). The colour lines are depth contours (Red: 5000m; Green: 4000m; Orange: 3000m; Cyan: 2000m; Blue: 1000m). The red dashed lines represent the open ocean boundaries.

The wind field and atmospheric pressure gradient field associated with a typhoon event are the principal drivers to generate wind waves and storm surge. In this study, the parametric models for both wind (Emanuel & Rotunno, 2011) and atmospheric pressure (Holland, 1980) fields are adopted. The models can satisfactorily reproduce the wind and pressure fields for Typhoon Hato event, provided that all the necessary input data for these parametric models are extracted from the typhoon's track information. The procedures for calculating the wind speed and pressure were well documented in Yang, et al. (2019), and will not be repeated here.

Since it is necessary to consider the tsunami source in the present study, the configurations of the coupled model are slightly different from those employed in Yang, et al. (2019). The main modifications are as follows: i) A smaller domain is employed in this study; ii) smaller grid sizes from the subduction zone towards the PRD are used; and iii) the boundary condition for tide is extracted from the FES2014 model. The usage of smaller grid sizes is necessary to ensure that the model can accurately capture the tsunami waves, since tsunami waves feature shorter wavelength than tide and storm surges. To ensure these modifications do not alter the quality of the results, the numerical hindcasting simulation of Typhoon Hato event is repeated, and the results are compared against the observations and the numerical results reported in Yang, et al. (2019). For brevity, readers can refer to Figure S1 in the supplementary materials for the details of comparisons. The verification procedure shows that the numerical model with the current configuration can reproduce the storm-tide event during Typhoon Hato, and the degree of accuracy of the new results is comparable to that reported in Yang, et al. (2019).

3.2 Tsunami generation and propagation

This study focuses on tsunamis generated by submarine earthquakes in the Manila subduction zone. Therefore, the displacement of the seafloor needs to be first calculated. The details of this technique for tsunami generation can be found in Sepúlveda (2017) and Sepúlveda, et al. (2017), and hence will not be repeated here. Figure 2(b) displays the seafloor displacement of the scenario chosen in this study. Stretching across the Luzon strait, the northern end of the rupture plane appears on the continental shelf at relatively shallow water depth of about a few hundred metres, and the southern end is located in deep water of a few thousand metres. The total length of the fault plane is about 550km. Its spatial distribution aligns with the shape of the Manila trench which is concave facing the China coastline. The maximum displacement is found to be more than 14m located near the mouth of Taiwan strait. This event is selected because the maximum seafloor displacement of this scenario is the largest among all 200 samples being generated. In order to obtain the initial free surface water level distribution from the seafloor movement, the following approximations are employed: (1) water is incompressible; (2) the seafloor vertical displacement is impulsive, i.e., the time scales of the slip and seafloor displacements are much shorter than that of the tsunami propagation; (3) the characteristic horizontal length of the seafloor deformation (hundreds of kilometres) is larger than water depths (a few kilometres); (4) the horizontal displacement of the seafloor does not contribute to the tsunami generation significantly. These simplifications lead to the conclusion that the water surface responds instantaneously to the seafloor motion and thus, the initial free surface elevation mimics the shape of seafloor vertical displacement (Bernard & Robinson, 2009; Sepúlveda, et al., 2017).

Before discussing the methodology for simulating the storm-tide-tsunami concurrent event, SCHISM is first used to simulate tsunami-alone scenario. To accomplish this, the SCHISM model is used without considering tide, wind or wind waves. At open ocean boundaries the free surface elevations are forced to be zero, which will generate very small waves as the tsunami waves reach the boundaries. However, these artificial waves are hardly noticeable (as seen in the Movie S1 provided in the supplementary materials). Moreover, in the present study, since only the first two leading tsunami waves recorded at Macau and Hong Kong are of interest, within this time frame, the artificial waves generated from the open boundaries are still far away from the coast and do not contaminate the leading tsunami waves. Therefore, no additional attempt has been made to improve this open boundary condition.

Three simulations have been performed with three different time-step sizes, 10s, 5s and 3s, representing different CFL numbers to ensure the convergence of the numerical results. The simulated time histories of water level around Hong Kong are compared with the numerical results based on COMCOT (Cornell Multi-grid Coupled Tsunami) model (Sepúlveda, et al., 2019) (personal communication). Good agreement among the present model results using different time step sizes and the solutions from COMCOT indicates that the present results are converged and accurate solutions. Therefore, the time

step size of 10s is sufficient for the purpose of this study. The details are omitted here for brevity, but they can be found in Figure S2 and S3 in the supplementary material.

3.3 Timing for triggering tsunami during typhoon event

As illustrated in the previous sections, the SCHISM-WWMIII package can reliably simulate a storm-tide event or a tsunami event, separately. However, since the objective of this study is to simulate a concurrent storm-tide-tsunami event, it is essential to introduce a procedure to trigger a tsunami during a typhoon event.

The procedure is rather straightforward and is described as follows. Since the typhoon event lasts a longer period than that of a tsunami event, the typhoon simulation is started first using the initial and boundary conditions and applying the atmospheric forcing as described in section 3.1. The water surface elevation and current velocity in SCHISM are updated every 10s and the directional spectra in WWMIII are updated every 600s. The two models are fully coupled and exchange data every 600s. During the simulation, the results are written to files every 60 time-steps in executing SCHISM or one time-step in executing WWMIII. These files are so-called "hot files", consisting of all the information to perform a hot start simulation. The frequency of producing "hot files", i.e., every 10 minutes, is chosen because it is much shorter than the storm surge process that lasts for many hours in coastal regions (Yang, et al., 2019). Hence, the storm-tide flow does not change dramatically within 10 minutes interval. If the tsunami is initiated at the n^{th} time step, the execution of SCHISM and WWMIII will be interrupted, and the initial free surface elevations representing the generated tsunami waves are added to the simulated free surface elevations at the n^{th} time step, which have been saved to the "hot files". Other physical quantities, e.g., the depth-averaged velocities and wave spectra, remain unchanged. The simulation is then restarted, continuing from the n^{th} time step until the end of the concurrent event. Readers can refer to the flow chart Figure S4 for the details about this procedure in the supplementary material.

This simple technique appears to be flexible and robust, allowing further experimenting with different tsunami initiation times so that coastal hazards can be assessed for various concurrent scenarios. The worst-case scenario in terms of coastal inundation at a specified site is when the leading tsunami wave crest and the storm-tide induced maximum water level arrive at the same time. More specifically, if the site of study is Macau, the required travel time of the leading tsunami from the tsunami source region to Macau can be estimated from the tsunami-alone simulation. Subtracting this time from the time when the maximum water level is recorded in the storm-tide-alone simulation yields the first guess for the tsunami initiation time.

However, this estimate may not ensure that the crest of the leading tsunami wave will arrive at the peak of the background water level, because the interactions between tsunami and storm-tide will modify the propagating speed of the tsunami. Nevertheless, this initial guess is helpful regarding the selection of the range of time steps to trigger the tsunami. An iterative procedure is used to show that the worst inundation scenarios are indeed selected correctly at Macau and Hong Kong. It is worth noting that the tsunami initiation time leading to the worst-case scenario at one site may not be the worst case at the other site. More details will be presented in the next section.

4 Results and discussions

In this section, the impacts of the concurrent storm-tide-tsunami scenarios in Macau and Hong Kong are investigated. A total number of 20 scenarios are considered, and in each scenario the tsunami is triggered at a specified timing between 06:00 and 09:10 on 23-Aug-2017 during the Typhoon Hato

event. Expressing in terms of the water level with respect to MSL (Mean Sea Level) the CM results can be written as (Bernard & Robinson, 2009; Winckler, et al., 2017)

$$\zeta^c = \zeta_{bg} + \zeta_t, \quad (1)$$

where ζ_t is the water level obtained from the tsunami-alone simulation, and ζ_{bg} is the water level corresponding to a typhoon (storm-tide) event, which are obtained as two separate simulations. On the other hand, we define the **Full Model (FM)** as the dynamical coupling of two hazards in one simulation, yielding the total surface elevation, ζ^f. Comparisons of the FM results against the CM results will be made so as to understand the efficacy of the CM for describing such concurrent events. The results in offshore region will be presented first in section 4.1, while results for coastal processes will be discussed in section 4.2. Finally, the inundation results in Macau and Hong Kong areas will be presented in section 4.3.

4.1 Water levels in offshore regions

In this section numerical results of offshore hydrodynamics, including the tsunami propagation process and the surface envelopes are presented. For clarity and brevity, only the results associated with the worst inundation scenario in Macau are reported here. The tsunami is triggered at 07:00 on 23-Aug-2017. Recall that the Typhoon Hato is still in progress and it makes the landfall at 12:50 on the same day. It is re-iterated here that this tsunami initiation time does not lead to the worst inundation in Hong Kong.

In Figure 4 ~ 7, snapshots of the free surface elevation distribution corresponding to (a) storm-tide-alone simulation (ζ_{bg}), (b) tsunami-alone simulatiom (ζ_t), and (c) storm-tide-tsunami simulation (ζ^f) are plotted for four instants (08:00, 09:00, 10:00 and 11:00 on 23-Aug-2017).

Figure 4(a) displays the surface elevations for storm-tide-alone scenario at 08:00 on 23-Aug-2017, 1 hour after the generation of the tsunami. The spatial variation of surface elevations is strongly dominated by the large tidal variations near the Taiwan Strait. However, Typhoon Hato has already generated measurable storm surges in the nearshore region. In Figure 4(b), the free surface elevations of the tsunami-alone scenario are shown. In the offshore region the water depth varies from over 5000 m in deep sea to a few hundred metres on the continental shelf, and the wave celerity of the leading tsunami wave decreases significantly on the continental break/shelf. Because of the dramatic change of the water depth in the vicinity of Dongsha island, tsunami waves are further diffracted by the island. Figure 4(b) shows that the diffracted wave front has already passed Dongsha island, showing the collision of two trapped waves at the lee side of the island. In front of the leading tsunami wave the sea surface is not disturbed. In Figure 4(c) the surface elevations for the concurrent storm-tide-tsunami are illustrated. Genarally speaking, significant interaction between tsunami waves and storm-tide only occurs in the low tide area near the southern end of Taiwan strait.

Similar to Figure 4, the free surface elevations for various scenarios at 09:00 on 23-Aug-2017, 2 hours after the incipient of the tsunamis, are shown in Figure 5. Figure 5(a) shows that at this hour, without considering tsunamis, the PRD region has already experienced high-tide, and the storm surge has also become noticeable. Figure 5(b) indicates that the leading tsunami waves have separated from Dongsha island and are propagating towards the China coastline, while the tsunami front is realigning itself with the bathymetry contours. The leading tsunami wave crest is followed by a clearly developed trough. Meanwhile, the trapped waves remain in the vicinity of Dongsha island with diminishing wave amplitudes. Figure 5(c) displays the free surface elevations for the concurrent storm-tide-tsunami event and shows that at this hour the tsunami wave is about to merge with the high tide near the PRD, and the tsunami wave is still farther away from PRD than the storm surge is.

Three hours after the initiation of tsunami waves, the storm surge becomes more evident in the vicinity of PRD, and the northeast part of the leading tsunami wave has also arrived at the coastal region as shown in Figure 6(a) and (b), respectively. The interactions among the high tide, tsunami, and storm surge enhance the overall water elevation near the mouth of PRD as seen in Figure 6(c). Figure 7 shows the free surface elevations at 11:00 on 23-Aug-2017, which is 4 hours after the earthquake and 2 hours before Typhoon's landfall. Note that the inundation has occurred in Macau at this hour as the inland water level gauges in the vicinity of Inner Harbour begins to pick up flooding water signal between 10:00~11:00 during the storm-tide event (Yang, et al., 2019). The storm surge and tide have brought significant increment to the water level on the west coast of PRD (Figure 7(a)), and the leading tsunami waves have also reached a much wider area of coast (Figure 7(b)). The interaction among high tide, storm surge, and tsunami wave leads to a significant increase of water level near the PRD region, which can be observed in Figure 7(c).

To evaluate the importance of dynamic interactions between storm-tide and tsunami, the differences between the results based on CM and FM, $\Delta\zeta = \zeta^c - \zeta^f$, at four instants (08:00, 09:00, 10:00 and 11:00 on 23-Aug-2017) are plotted in Figure 8. It is recalled here that in the FM (ζ^f) full interactions between tsunami waves, storm surge and tide are simulated. On the other hand, in the CM the interactions of these processes are completely ignored, and the CM results are the summation of the storm-tide-alone simulation (ζ_{bg}) and the tsunami-alone simulation (ζ_t). Significant differences, $\Delta\zeta$, can be observed on the continental shelf during the first two hours after the initiation of the tsunamis (Figure 8(a) and (b)). The discrepancy is primarily caused by the modification of the wave celerity and the propagation direction of tsunami waves due to the appearance of tides and storm surge, which have a longer time and length scales than that of tsunami waves. Thus, the patterns of large differences in the water level are closely correlated with the leading tsunami wave heights (Figure 8(a) and (b)). The differences grow as the tsunami waves approaching the coast (Figure 8(c) and (d)), where the nonlinear interactions become more important. Another factor that contributes to the difference between the CM and the FM results is that the wind stress also affects tsunami waves in the FM, whereas it is overlooked in the CM.

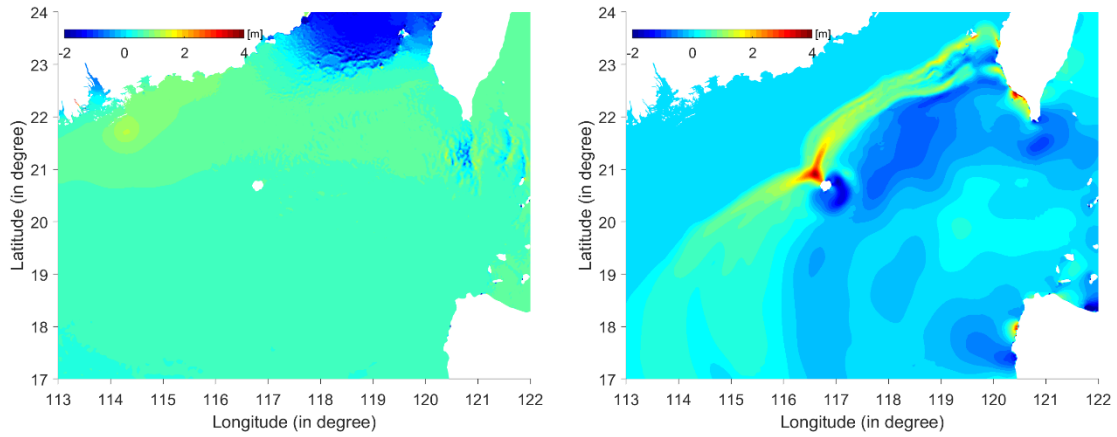

(a) Storm-tide-alone simulation (ζ_{bg})

(b) Tsunami-alone simulatiom (ζ_t)

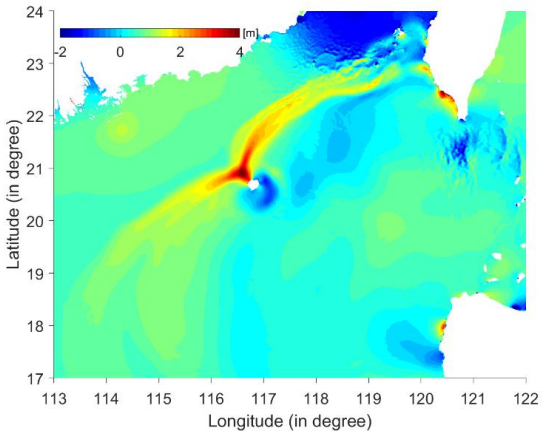

(c) Storm-tide-tsunami event by FM (ζ^f)

Figure 4. Snapshots of the free surface elevation with respect to MSL at 08:00 on 23-Aug-2017. A tsunami is triggered at 07:00 on the same day. Graded colour denotes the magnitude of the surface elevation in metres and white colour indicates land, where PRD is on the top left corner and Dongsha island is in the middle of the domain, Taiwan is on the top right corner and Philippines is on the bottom right corner.

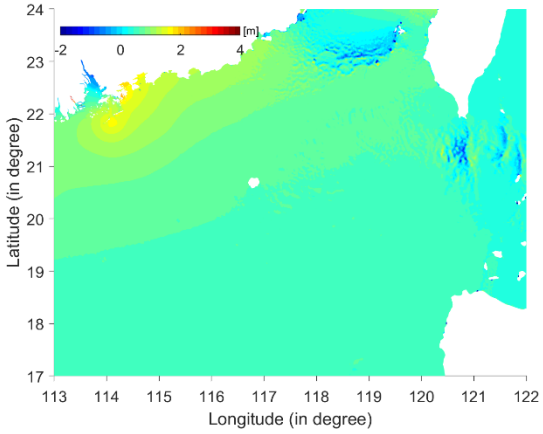

(a) Storm-tide-alone simulation (ζ_{bg})

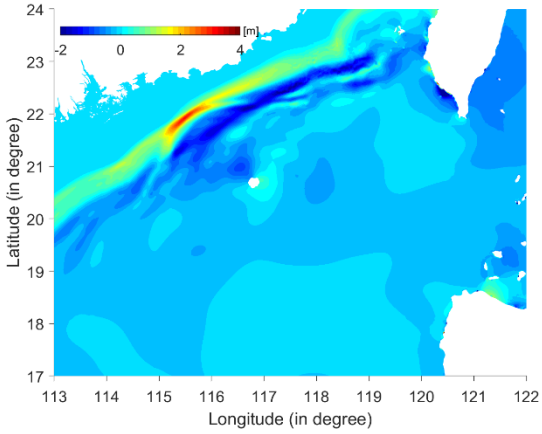

(b) Tsunami-alone simulation (ζ_t)

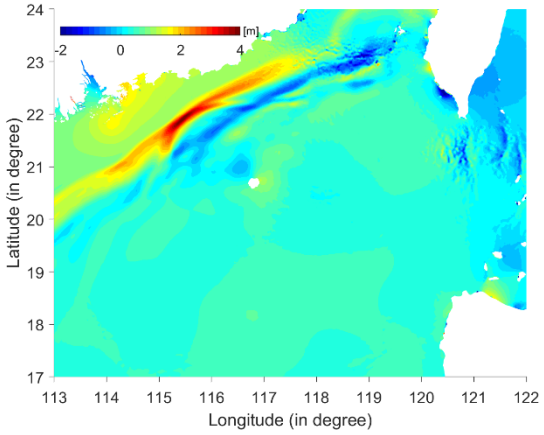

(c) Storm-tide-tsunami event by FM (ζ^f)

Figure 5. Snapshots of the free surface elevation with respect to MSL at 09:00 on 23-Aug-2017. See figure caption of Figure 4.

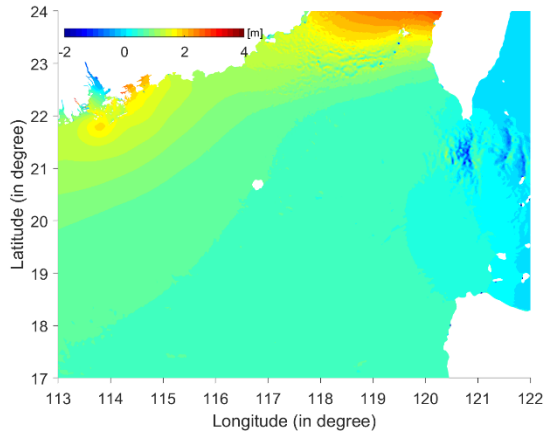

(a) Storm-tide-alone simulation (ζ_{bg})

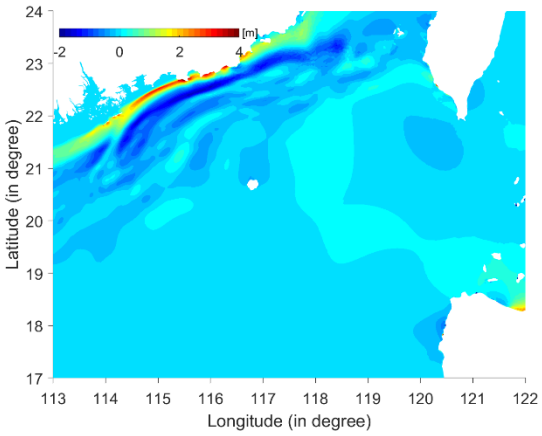

(b) Tsunami-alone simulation (ζ_t)

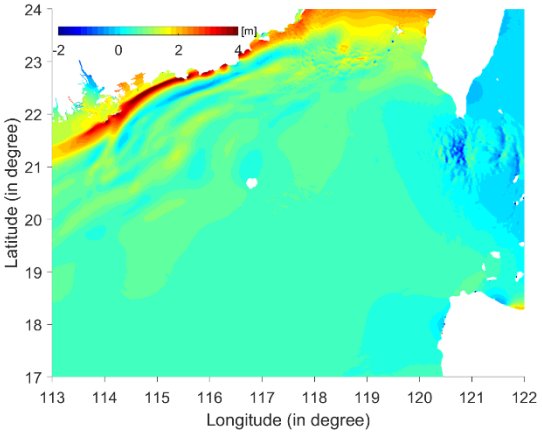

(c) Storm-tide-tsunami event by FM (ζ^f)

Figure 6. Snapshots of the free surface elevation with respect to MSL at 10:00 on 23-Aug-2017. See figure caption of Figure 4.

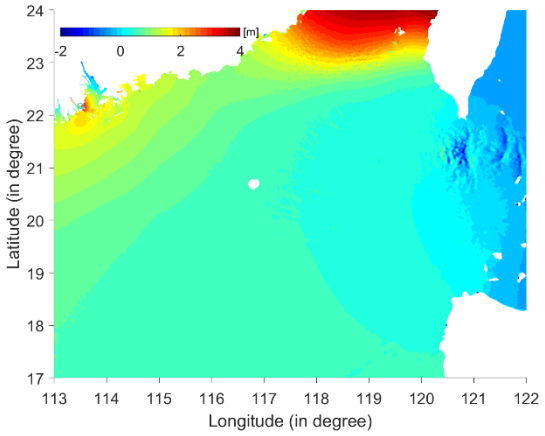

(a) Storm-tide-alone simulation (ζ_{bg})

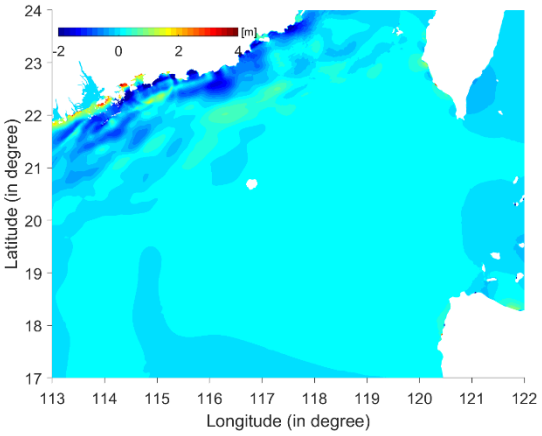

(b) Tsunami-alone simulation (ζ_t)

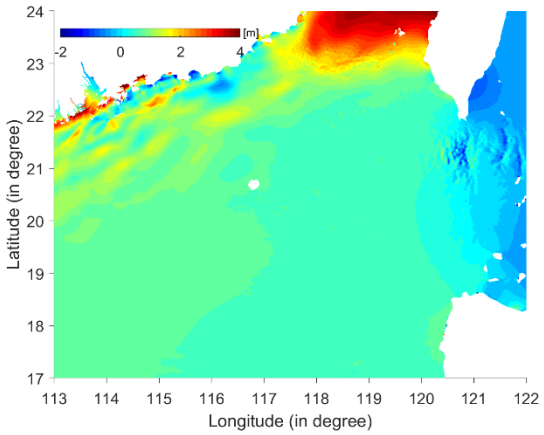

(c) Storm-tide-tsunami event by FM (ζ^f)

Figure 7. Snapshots of the free surface elevation with respect to MSL at 11:00 on 23-Aug-2017. See figure caption of Figure 4.

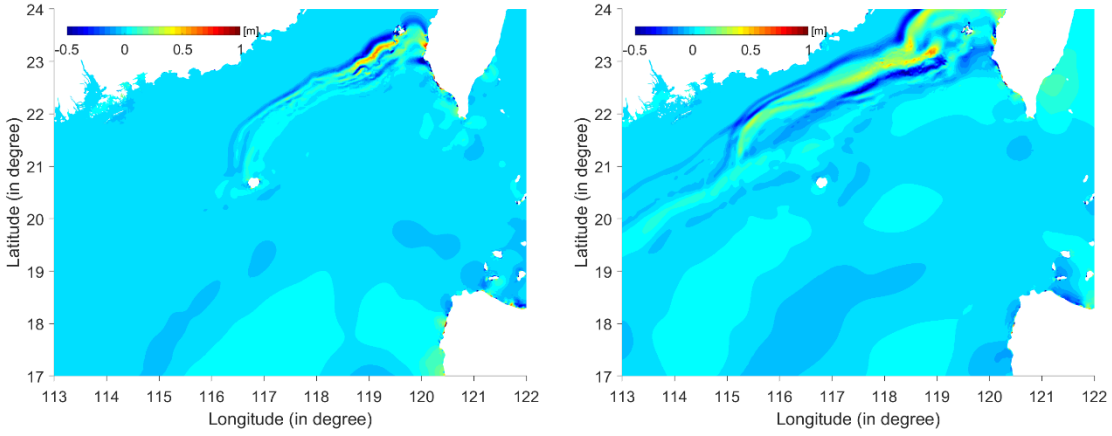

(a) $\Delta\zeta$ after 1 hour

(b) $\Delta\zeta$ after 2 hours

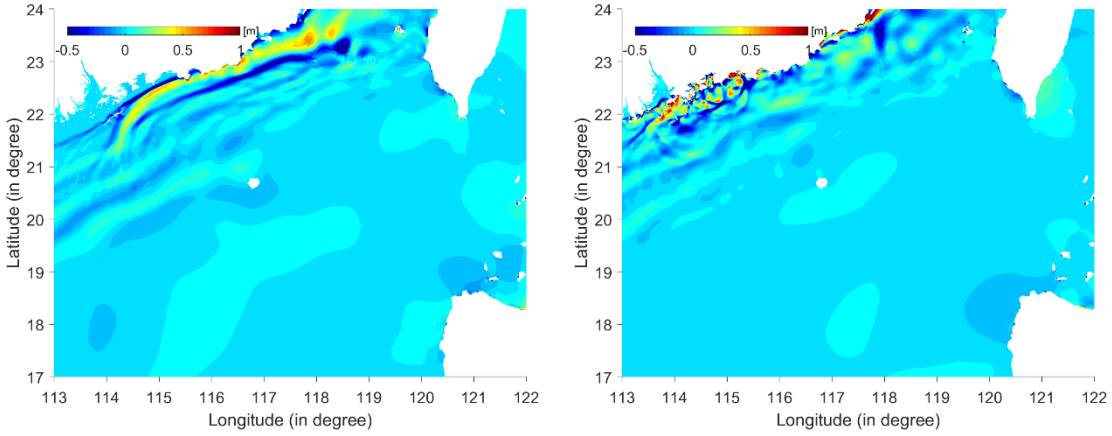

(c) $\Delta\zeta$ after 3 hours

(d) $\Delta\zeta$ after 4 hours

Figure 8. Differences of instantaneous surface elevation between the CM and the FM results, $\Delta\zeta$, for the storm-tide-tsunami scenario. Time starts at the initiation of tsunami.

To further illustrate the effects of storm-tide on tsunami waves, the envelope of maximum water surface elevation throughout the entire event duration, and the corresponding arrival times are shown in Figure 9 (a) and (b) for the tsunami-alone scenario and the storm-tide-tsunami scenario, respectively. In the case of tsunami-alone simulation (Figure 9(a)), the maximum water surface elevation coincides with the leading wave crest. This tsunami feature has been identified by Okal & Synolakis (2016) as the so-called "maximum first" pattern. In the storm-tide-tsunami simulations (Figure 9(b)), the arrival times of the maximum water surface elevation basically agrees with the locations of the leading tsunami wave crest as shown in Figure 4(c) ~ Figure 7(c) as well, except at Taiwan Strait where the maximum water level is dominated by high tide. Moreover, as depicted in Figure 9(a) the propagation direction of the leading tsunami crest line turns to its right due to refraction, i.e., the northern end of crest line subjects to a deceleration due to the reduction of water depth. Contour lines of the arrival time of the maximum water level do not change very much in the concurrent storm-tide-tsunami simulation as seen in Figure 9(b). It can also be found in Figure 9(a) that the most energetic part of the tsunami (the darkest colour) propagates towards the east side of the PRD. This phenomenon of energy focusing is also observed in the concurrent storm-tide-tsunami simulation (Figure 9(b)). Meanwhile, an enhancement to the maximum water level can also be seen in the vicinity of Macau on the west of PRD in the storm-tide-tsunami simulation (Figure 9(b)). This is mainly due to the appearance of storm surge superimposed on high tide (see Figure. S5 in the supplementary material). Thus, it can be concluded that the tsunamis have more significant impacts on Hong Kong than Macau, and on the other hand, the Hato-like typhoon causes more significant flooding in Macau than Hong Kong, which will be further discussed when the tsunami heights recorded at tidal gauges are discussed in a later section.

The differences in the maximum water surface elevations and their arrival times obtained from the CM and the FM are presented in Figure 10, focusing only in the vicinity of PRD. Figure 10(a) shows that in general the CM underpredicts the maximum water surface elevation in comparison with the FM's results, and the difference is more than 1m. In addition, at the mouth of Pearl River, the CM also reports delayed arrival times of the maximum water surface elevation by more than 10 mins as compared with those predicted by the FM. These differences are primarily caused by the modification of the wave celerity and the propagation direction of tsunami waves due to the appearance of tides and storm surge as pointed out in Figure 8. It is re-iterated here that in the FM the tsunami waves are also subject to atmospheric forcing, since tsunami waves are simulated together with storm surge and tides in SCHISM. Consequently, the FM results in the nearshore region are anticipated to differ significantly from those obtained from the CM, which will be discussed in the next section.

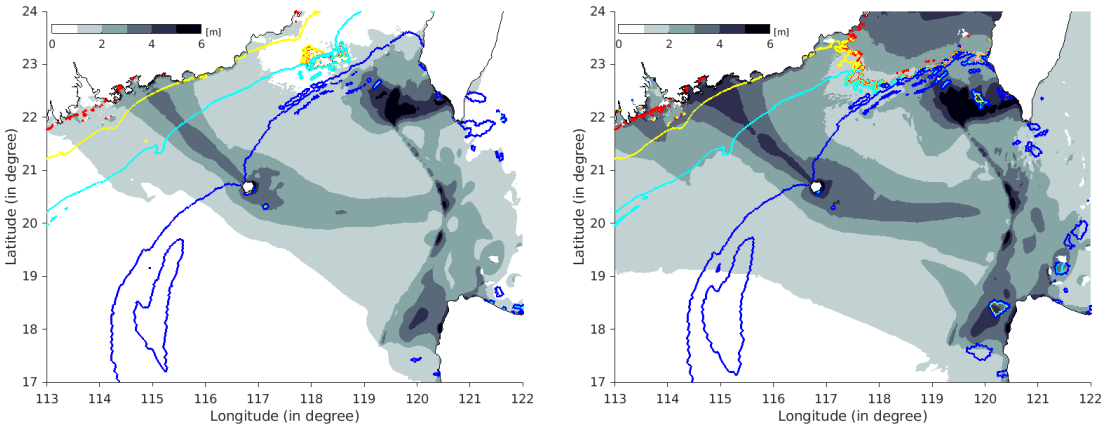

(a) Tsunami-alone simulation (b) Storm-tide-tsunami simulation

Figure 9. Map of the maximum water surface elevations and the corresponding arrival times. (a) Tsunami-alone simulation and (b) the storm-tide-tsunami simulation (FM). Colour indicates the water surface elevation

measured from MSL in metres and contour lines represent their arrival times in hour. The time clock starts at the initiation of tsunami. Blue line: 1-hour contour; cyan line: 2-hours contour; yellow line: 3-hours contour; red line: 4-hours contour.

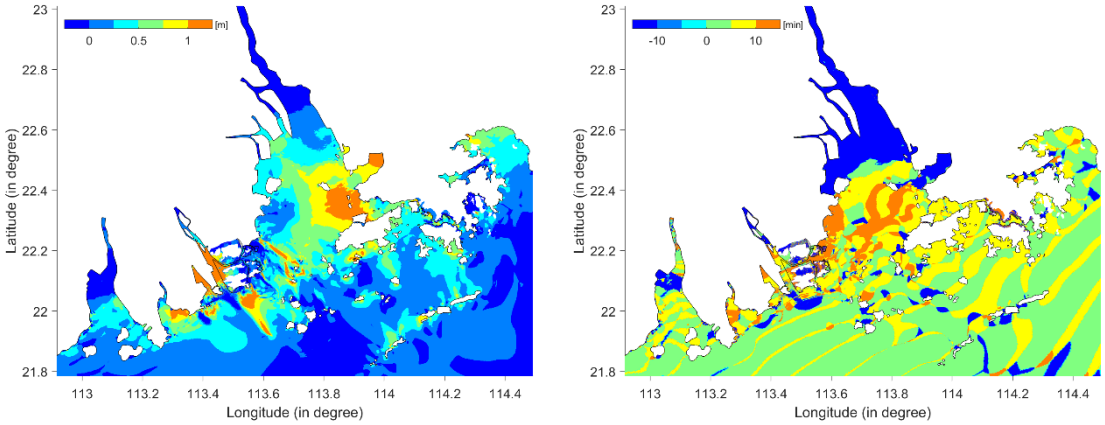

(a) Difference in maximum water surface elevation (b) Difference in arrival time

Figure 10. Differences of the maximum water surface elevations and the corresponding arrival times between CM and FM results. (a) The difference in maximum water surface elevation; the colour scale is in metre; (b)the difference in the corresponding arrival time; the colour scale is in minute.

4.2 Coastal processes

4.2.1 Envelope of maximum water surface elevation

The envelopes of water levels in the vicinity of Macau and Hong Kong for the same scenario as that presented in the previous section, i.e., the tsunami is triggered at 07:00 on 23-Aug-2017, are calculated. Recall that this timing for tsunami generation leads to the worst inundation scenario for Macau, not for Hong Kong. The worst inundation scenario for Hong Kong will be reported separately in section 4.3. Figure 11 and Figure 12 display the maximum water surface elevations in the vicinity of Macau and Hong Kong, respectively, using (a) storm-tide-alone simulation, (b) tsunami-alone simulation, and (c) storm-tide-tsunami simulation by the FM. In Figure 11(d) and Figure 12(d) the differences of the surface envelope heights between the CM and the FM are also shown.

Overall, the impact of tsunami-alone in Macau is relatively low. With the exception of the small area at the southern tip of Coloane coast, maximum tsunami wave heights are less than 1.5m in the coastal water of Macau (Figure 11(b)). On the other hand, the maximum water levels associated with the storm-tide event are relatively high. As shown in Figure 11(a), the maximum water levels are 3.8m~4m around Inner Harbour. When the concurrent event is considered as shown in Figure 11(c), the maximum water levels reach 6.5m~7m along the south coast of Coloane, 5.5m~6.5m in the northeast coast of Macau, and 4.5m ~ 5m within the Inner Harbour area. They are much higher than the corresponding water levels induced by the storm-tide-alone event and the tsunami-alone event. Finally, Figure 11(d) shows that the CM underpredicts the maximum water level heights for 1m~1.5m in the southeast coast of Coloane and 0.5m~1m in the northeast coast of the Peninsula. However, it overestimates the maximum water level height for 0~0.5m inside the Inner Harbour.

Since Hong Kong is much bigger in size compared with Macau, only the Kai Tak terminal's adjacent area is investigated, given the importance of this area as the commercial centre of Hong Kong and its close proximity to the Victoria Harbour. The vulnerability of this area under tsunamis impacts has been demonstrated in Sepúlveda, et al. (2019). Intuitively, the concurrent storm-tide-tsunami is anticipated

to cause much severer damage to this area than by tsunami-alone or storm-tide-alone events. Figure 12(a) and (b) show that the storm-tide-alone event induces about 1.5m~2m maximum water levels throughout this region, whereas the tsunami-alone event causes maximum water levels of 3.5m~4m in Junk Bay and 3m~3.5m in Kowloon Bay. As shown in Figure 12(c) for the concurrent storm-tide-tsunami simulation, maximum water levels of 5m~5.5m are detected in Junk Bay, 4m~5m in Kowloon Bay, and 3m~4.5m at Lei Yue Mun and Victoria Harbour. Moreover, Figure 12(d) reveals that the CM overpredicts the envelope for 0.5m~1m near Lei Yue Mun and Victoria Harbour, whereas the difference between results of CM and FM is in the range of -0.25m~0.75m in the vicinity of Junk Bay and Kowloon Bay.

Regarding the differences between CM and FM results, there is a major difference in the results for Macau and Hong Kong. Specifically, in Macau large differences between results of CM and FM appear at the locations associated with the large envelop height. On the contrary, in the vicinity of Kai Tak terminal region, the differences between the results of CM and FM are relatively small at locations where large envelope heights are observed. Instead, they occur at locations where the envelope heights are relatively small, however, velocities are large (see Figure 12(e)). It is found that strong velocities and vortices are detected at these locations, which will be further discussed in subsection 4.2.3. The association of the differences between results of CM and FM and the distribution of surface elevation and velocity envelopes in space needs to be investigated comprehensively, however, it is not the focus of this study so will not be further discussed here.

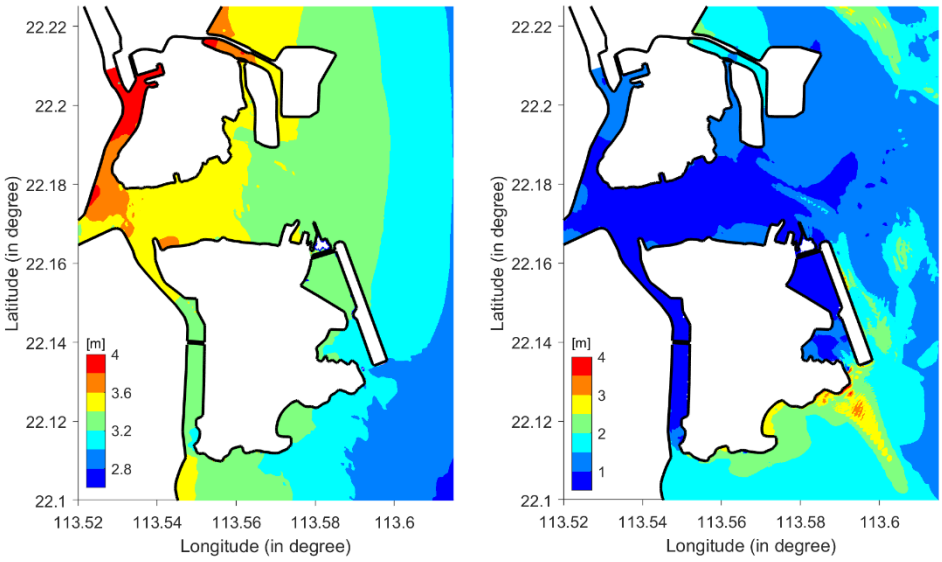

(a) Storm-tide-alone simulation

(b) Tsunami-alone simulation

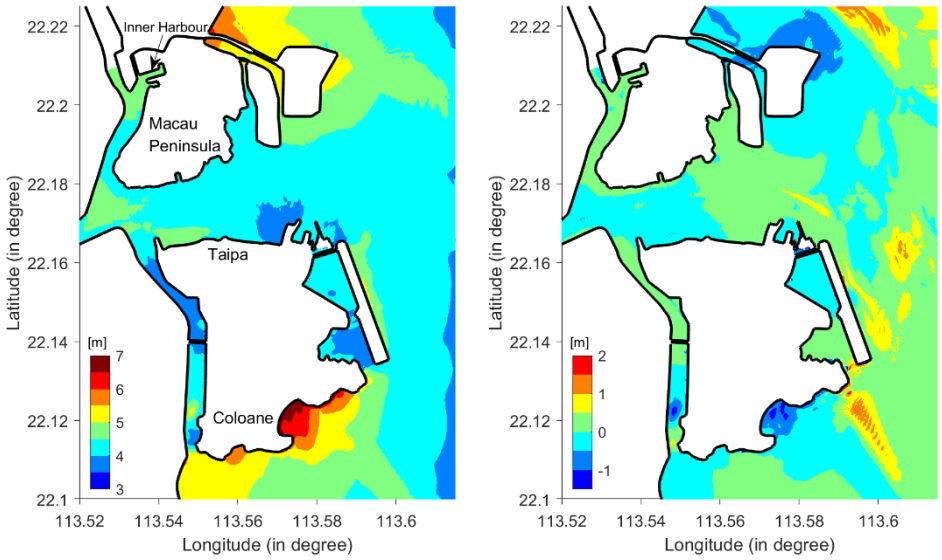

(c) Storm-tide-tsunami event by FM, $\max\{\zeta^f\}$ (d) $\max\{\zeta^c\} - \max\{\zeta^f\}$

Figure 11. Envelopes of water surface elevations in Macau for (a) storm-tide-alone simulation, (b) tsunami-alone simulation, and (c) concurrent storm-tide-tsunami simulation, $\max\{\zeta^f\}$. (d) Differences of the water elevation envelope between CM ($\max\{\zeta^c\}$) and FM ($\max\{\zeta^f\}$) results.

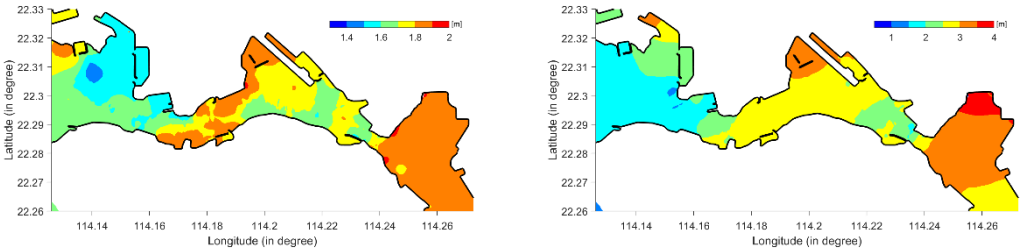

(a) Storm-tide-alone simulation (b) Tsunami-alone simulation

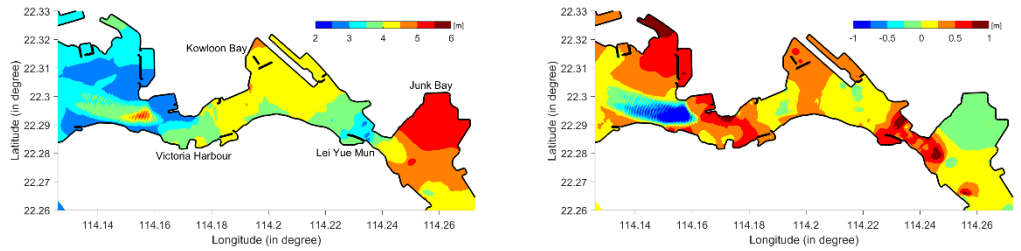

(c) Storm-tide-tsunami event by FM $\max\{\zeta^f\}$ (d) $\max\{\zeta^c\} - \max\{\zeta^f\}$

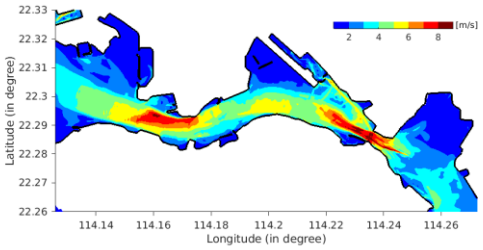

(e) Storm-tide-tsunami event by FM max{$|\boldsymbol{u}|^f$}

Figure 12. Envelopes of water surface elevations in the Kai Tak terminal adjacent region in Hong Kong for (a) storm-tide-alone simulation, (b) tsunami-alone simulation, and (c) concurrent storm-tide-tsunami simulation, max{ζ^f}. (d) Differences of the water elevation envelope between CM (max{ζ^c}) and FM (max{ζ^f}) results. (e) Velocity envelope for concurrent storm-tide-tsunami simulation, max{$|\boldsymbol{u}|^f$}

4.2.2 Peak water level height and arrival time based on tidal gauge signals

The numerically simulated time series of water surface elevations at several tide gauge stations are analysed. The locations of these stations are shown in Figure 1. The time histories of water surface elevation obtained from the storm-tide-alone simulation, tsunami-alone simulation and concurrent storm-tide-tsunami simulations based on FM and CM are summarised in Figure 13. It is re-iterated that the tsunami is triggered at 07:00 on 23-Aug-2017. For brevity, only two stations, i.e., Dahengqin near Macau and Quarry Bay in Hong Kong, are selected for discussions here. The results at other stations are presented in the supplementary materials (see Figure S6). As shown in Figure 13, the storm-tide water level at Dahengqin is substantially higher than that recorded at Quarry Bay. On the contrary, the peak height of tsunamis at Quarry Bay is much higher than that at Dahengqin.

As shown in Figure 13(a), the maximum water level at Dahengqin is 3.75m for the storm-tide-tsunami simulation based on the FM, and the leading tsunami crest arrives earlier in the FM simulation. The CM model underestimates the maximum water level by about 0.1m. It can be said that the interactions between the storm-tide and tsunamis have enhanced the maximum water level in the FM simulation at Dahengqin station. The time histories of water levels at Quarry Bay are shown in Figure 13 (b), indicating that the maximum water level is 3.62m for the storm-tide-tsunami simulation based on the FM. It is noticed that similar to Dahengqin, the tsunamis arrive earlier in the FM results. However, the CM has a higher water level for about 0.22m.

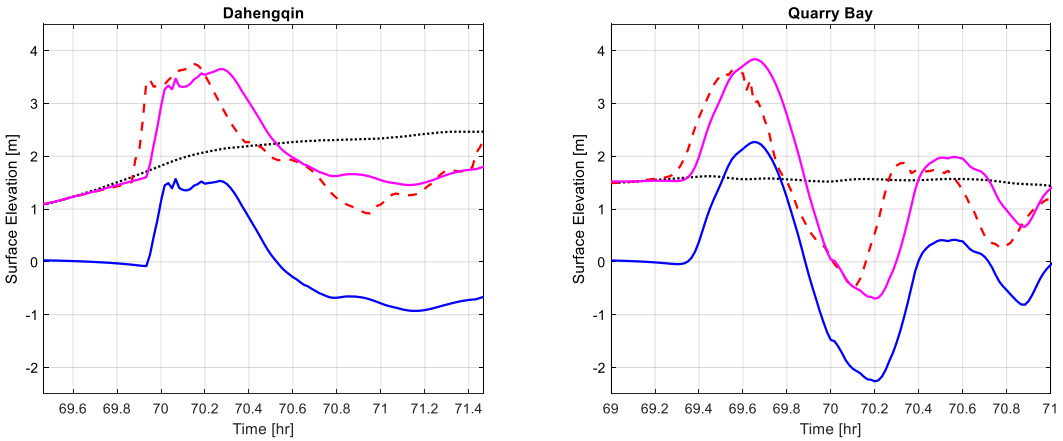

(a) Dahengqin (b) Quarry Bay

Figure 13. Time histories of water surface elevation recorded at tide gauges. Black "····": storm-tide-alone simulation (ζ_{bg}); blue "—": tsunami-alone simulation (ζ_t); red "— —": storm-tide-tsunami simulation results based on FM (ζ^f); magenta "—": storm-tide-tsunami simulation results based on CM (ζ^c). Abscissa is the time from the start of the simulation in hour, ordinate denotes surface elevation in metres.

The differences between the CM and FM results in terms of the maximum water surface elevation and its arrival time (the time interval from the initiation of tsunami to when the maximum water level is recorded) depend on the selected site location and the tsunami initiation timing. In Figure 14 the FM ($\max\{\zeta^f\}$, $t_{\max\{\zeta^f\}}$) and CM ($\max\{\zeta^c\}$, $t_{\max\{\zeta^c\}}$) values at all tide gauge stations (see Figure 1) using different tsunami initiation times (from 06:00 ~ 09:10 on 23-Aug-2017) are plotted together. Figure 14(a) shows that the highest maximum water surface elevation is observed at Sanzao of about 4.7m and smallest at Chiwan of about 1.9m. Furthermore, it is found that the maximum water levels predicted by the FM can be 0.88~1.17 times of those by the CM within the confidence interval of 90%. On the other hand, Figure 14(b) depicts that the arrival time of the maximum water surface elevation can be as early as 2.4 hours after the initiation of tsunamis at Macau (dominated by storm-tide), while it can be as late as 8.6 hours at Hengmen. Overall, the arrival time predicted by the FM is 0.87~1.18 times of the CM results. In summary, the differences between the results by using the FM and CM are site-specific and also vary with the tsunami initiation timing. This is understandable as the interaction between tsunamis and background process depends highly on the bathymetries, coastline configurations, relevant strength of tsunamis and tidal forcing, as well as the interplay among tidal phases, momentum flux and bottom friction (Kowalik & Proshutinsky, 2010).

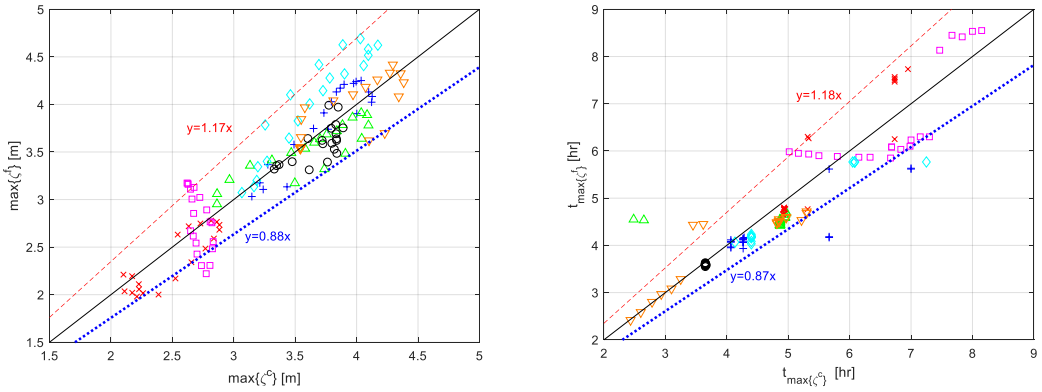

(a) Peak water levels (b) Peak arrival time

Figure 14. Comparisons of the maximum water surface elevations and their arrival time between CM and FM results. Red dash and blue dot lines indicate the upper and lower bounds, respectively, of the 90% confidence interval. Blue "+": Dahengqin; green "△": Zhuhai; red "X": Chiwan; pink "□": Hengmen; cyan "◊": Sanzao; black "○": Quarry Bay; orange "▽": Macau. (See Figure 1 for their locations).

4.2.3 Instantaneous velocity vector field

Quantification of the nearshore velocity magnitudes and directions is important in assessing coastal hazards. To visualize the spatiotemporal variation of the flow patterns during the concurrent storm-tide-tsunami events, the depth-averaged velocity field is extracted in the neighbourhood of Macau and Kai Tak terminal adjacent region in Hong Kong. The simulated scenario corresponds to the worst inundation in Macau with tsunami being initiated at 07:00 on 23-Aug-2017. The velocity field in the vicinity of

Macau at 11:30 and 12:20 on 23-Aug-2017 for the storm-tide-alone, tsunami-alone and concurrent storm-tide-tsunami simulations by using the FM are shown in Figure 15 and Figure 16, respectively. On the other hand, the velocity fields in Kai Tak terminal adjacent region in Hong Kong at 10:40 and 11:20 are extracted and displayed in Figure 17 and Figure 18, respectively.

As discussed previously, Macau is more affected by the storm-tide. Figure 15(a) shows that during the storm-tide event a strong current is generated across the channel between Macau Peninsula and Taipa at 11:30. This flow is divided into two streams. One moves towards the Inner Harbour and the other into Maliuzhou Waterway. The velocity within the Inner Harbour reaches 2~2.5m/s. Meanwhile, as shown in Figure 15(b), in the tsunami-alone scenario the tsunami wave front arrives at the entrance of the channel, and the area in front of the tsunamis is not disturbed. However, the results of concurrent storm-tide-tsunami simulation indicates that the storm-tide and tsunamis have merged into a stronger flow across the channel (Figure 15(c)). The flow velocity within Inner Harbour is enhanced to 3~3.5m/s. At 12:20, the flood within the Inner Harbour starts to retreat in the storm-tide-alone simulation as shown in Figure 16(a). The outgoing flow in the Inner Harbour reaches 3.5~4m/s. At the same time, the arrival of the tsunamis trough induces an offshore flow in the east of Macau in the tsunami-alone simulation as shown in Figure 16(b). The results of the instantaneous velocity field around Macau suggest that the superposition of the storm-tide and tsunamis can enhance the flow within the Inner Harbour area compared with storm-tide-alone and tsunami-alone simulations.

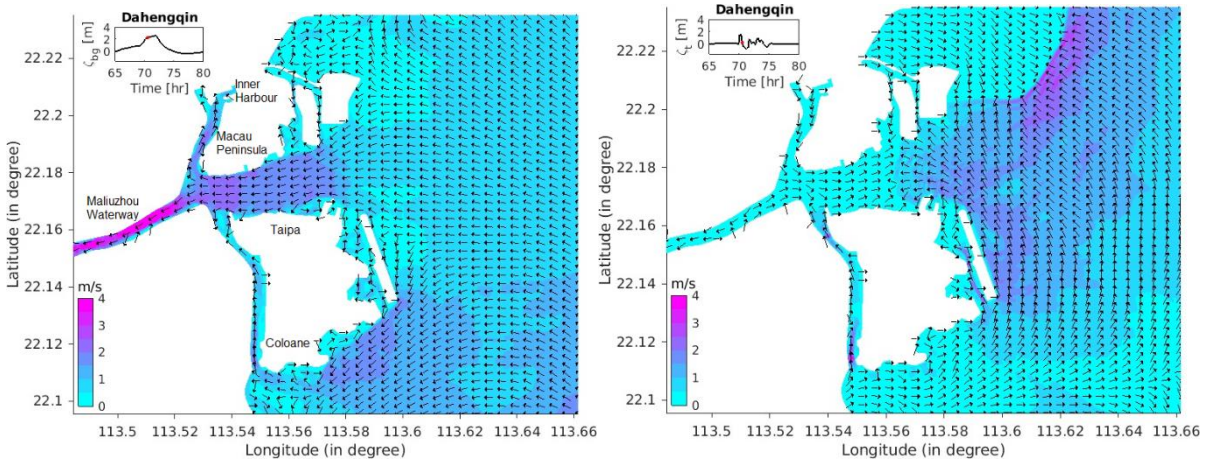

(a) Storm-tide-alone simulation ($\boldsymbol{u}_{bg}$) (b) Tsunami-alone simulation ($\boldsymbol{u}_{t}$)

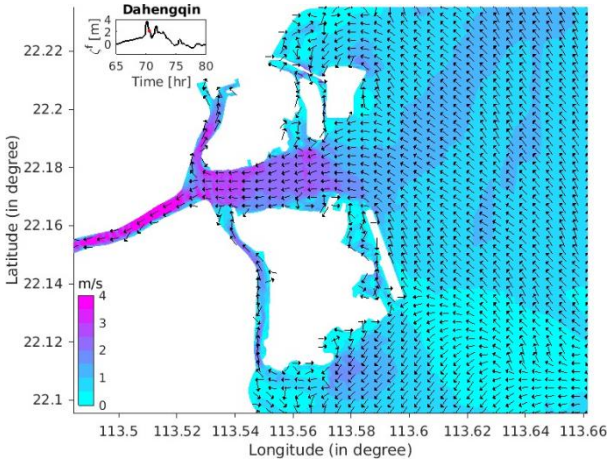

(c) Storm-tide-tsunami simulation by FM ($\boldsymbol{u}^{f}$)

Figure 15. Flow patterns in the vicinity of Macau at 11:30 on 23-Aug-2017. Colour indicates the magnitude of the depth-averaged velocity in m/s, and arrows represent velocity directions. The embedded subfigure is the time history of surface elevation at Dahengqin station, while the red dot indicates the time instant of the snapshots. Its abscissa denotes the time in hour from the start of the simulation and ordinate indicates the surface elevation in metres.

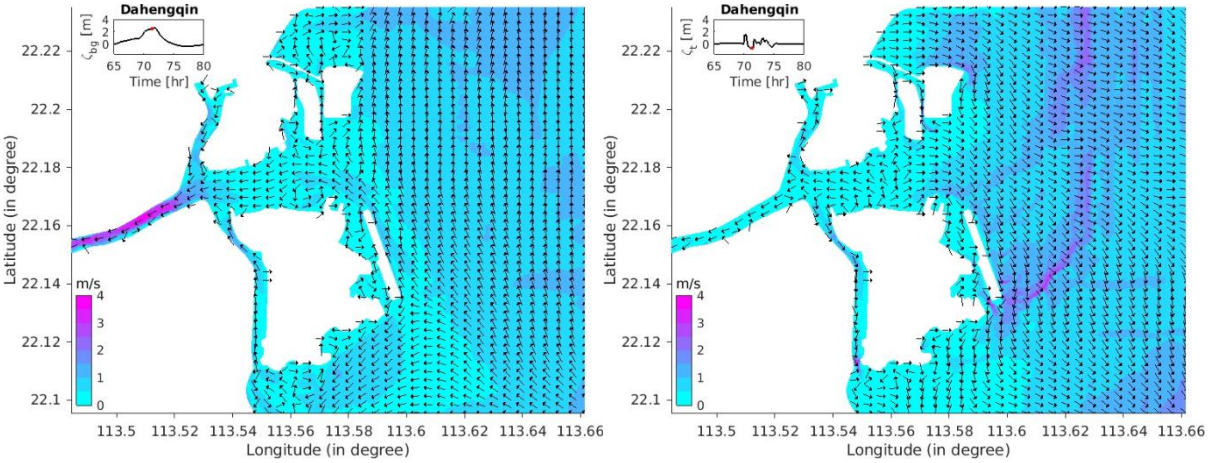

(a) Storm-tide-alone simulation ($\boldsymbol{u}_{bg}$) (b) Tsunami-alone simulation ($\boldsymbol{u}_{t}$)

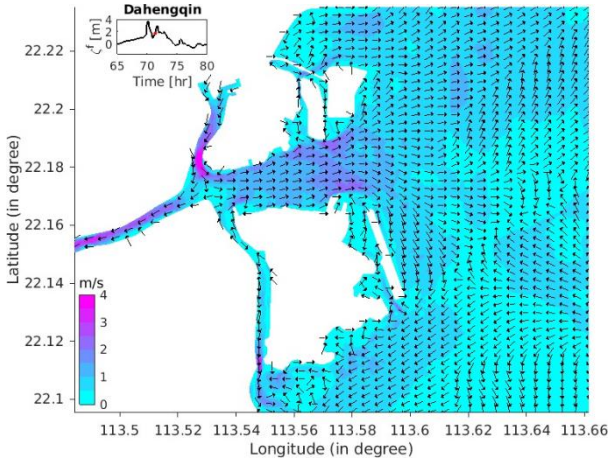

(c) Storm-tide-tsunami simulation by FM ($\boldsymbol{u}^{f}$)

Figure 16. Flow patterns around Macau at 12:20 on 23-Aug-2017. See figure caption of Figure 15.

The neighbourhood of Kai Tak terminal in Hong Kong experiences strong east-to-west flows at 10:40 in both storm-tide-alone and tsunami-alone scenarios as shown in Figure 17(a) and (b), respectively. In the concurrent storm-tide-tsunami event, the flows in the channel are enhanced and the velocity reaches 5.5~6.5m/s at Lei Yue Mun, Kowloon Bay and Victoria Harbour (Figure 17(c) and (d)). The prominent feature observed at this instant is the formation of a large vortex near Lei Yue Mun. It is not found in the storm-tide-alone or tsunami-alone simulations, since in the concurrent event the flow is enhanced at the narrow entrance of Lei Yue Mun and the maximum Reynolds number (defined as the ratio of cross-section mean velocity times hydraulic radius over the kinematic viscosity) can reach 1.9×10^{8} at the narrowest opening. Attributed to the large velocity, the flow transits to turbulence leading to the appearances of vortices (Figure 17(d)). At 11:20, the flows inside the channel remain in the westward direction for the storm-tide-alone event (Figure 18(a)). However, for the tsunami-alone event the flow changes its direction, pointing eastwards as depicted in Figure 18(b), and the magnitude of the velocity

reaches 5.5~6m/s, which is much stronger than that in storm-tide-alone scenario simulation. As shown in Figure 18(c), a west-to-east flow is formed within the channel in the concurrent storm-tide-tsunami simulation. The direction of the flow implies that the tsunamis might play a dominating role in this region. However, owing to the opposite direction of storm-tide flow and tsunamis flow, the net flux cancels out, resulting in a relatively weak current velocity of about 4~4.5m/s in this channel. The most distinguishable feature of the flow patterns in the Kai Tak terminal adjacent region is the formation of vortices near Lei Yue Mun. Note that this location is also where a large difference between FM and CM results is observed.

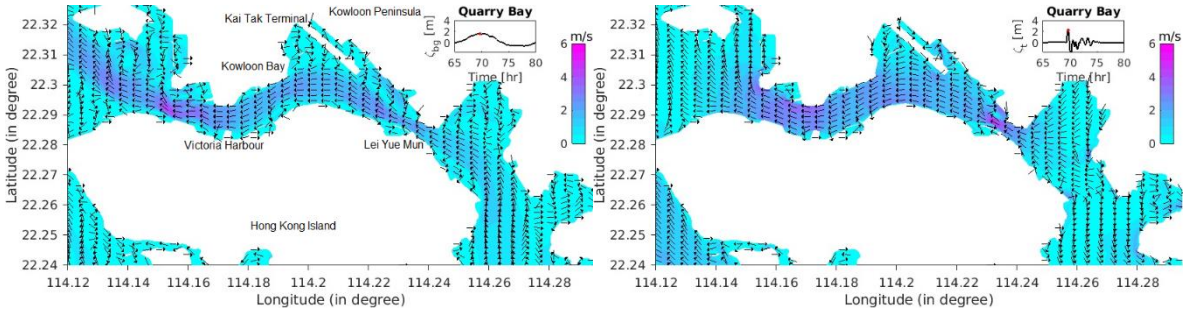

(a) Storm-tide-alone simulation ($\boldsymbol{u}_{bg}$) (b) Tsunami-alone simulation ($\boldsymbol{u}_t$)

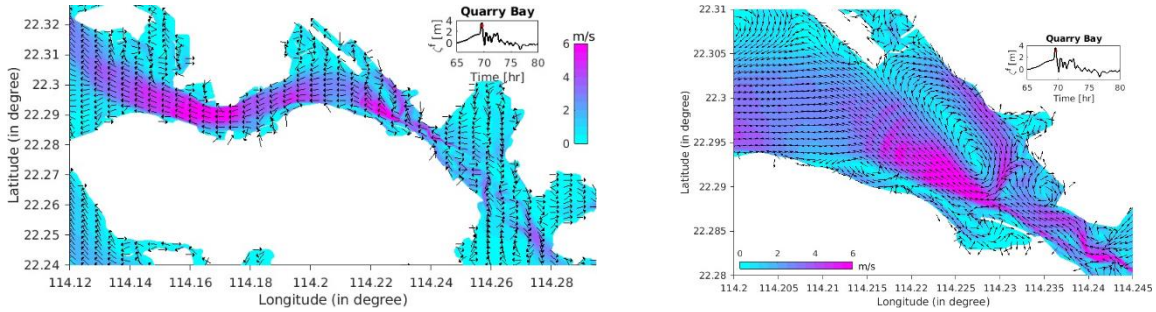

(c) Storm-tide-tsunami simulation by FM ($\boldsymbol{u}^f$) (d) Zoom-in to west of Lei Yue Mun for Panel (c)

Figure 17. Flow pattern in the vicinity of Kai Tak terminal in Hong Kong at 10:40 on 23-Aug-2017. Colour indicates the magnitude of the depth-averaged velocity in m/s, and arrows are for velocity direction. The embedded subfigure is the time history of the surface elevation at Quarry Bay station, while the red dot indicates the present time instant. Its abscissa denotes the time in hour from the start of the simulation and ordinate indicates the surface elevation in metre.

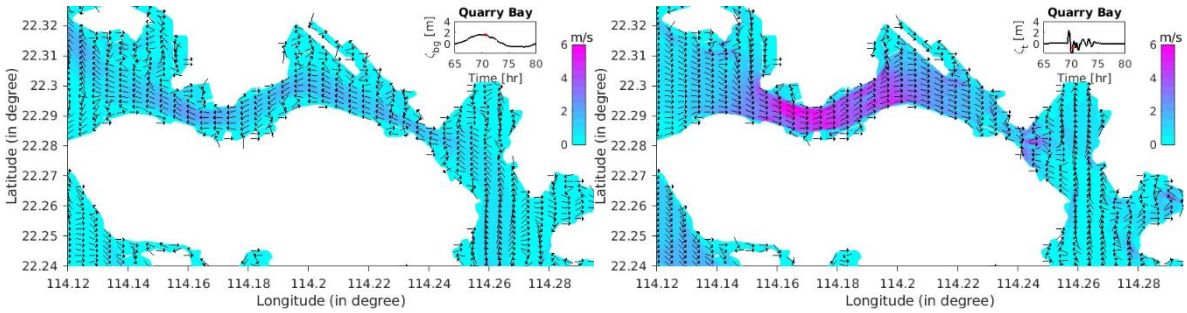

(a) Storm-tide-alone simulation ($\boldsymbol{u}_{bg}$) (b) Tsunami-alone simulation ($\boldsymbol{u}_t$)

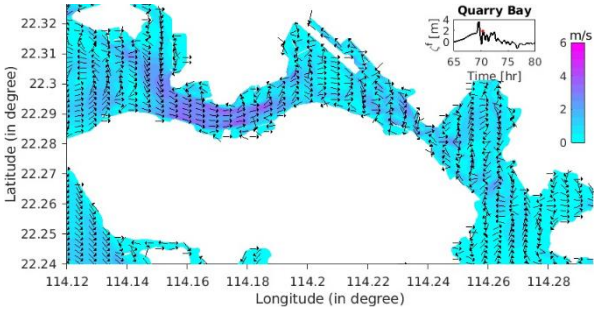

(c) Storm-tide-tsunami simulation by FM ($\boldsymbol{u}^{(f)}$)

Figure 18. Flow patterns in the vicinity of Kai Tak terminal region in Hong Kong at 11:20 on 23-Aug-2017. See the figure caption of Figure 17.

4.3 Inundation depth and duration

To demonstrate the severity of inundation, the maximum inundation depths (water depth above the ground level) for the storm-tide-alone scenario, tsunami-alone scenario, and the concurrent storm-tide-tsunami scenario by using the FM, respectively, are plotted for Macau and Kai Tak terminal region in Hong Kong in Figure 19 and Figure 20, respectively. The threshold of inundation depth for estimating the flood duration is selected as 0.5m, because an adult will lose his balance standing in flood water depth higher than this value corresponding to 1.2m/s flow velocity (Martínez-Gomariz, et al., 2016). The corresponding inundation durations are also calculated for the concurrent storm-tide-tsunami scenario.

As shown in Figure 19(a), the storm-tide-alone scenario induces substantial flooding in the Inner Harbour area. The inundation depth and extent are similar to those reported in Yang, et al. (2019), which have been validated against the post-typhoon survey data. It is found that the inundation depth can be of 2 ~ 2.5m along the Inner Harbour coast and 1.5 ~ 2m on the east of the harbour. The rest of Macau is not affected by the flood in the storm-tide-alone scenario simulation. Meanwhile, Figure 19(b) shows that the tsunami-alone scenario does not cause measurable inundation in Macau. On the contrary, the concurrent storm-tide-tsunami scenario not only inundates the Inner Harbour area, but also the east coast of Macau Peninsula, including the two artificial islands as shown in Figure 19(c). The inundation water depth reaches 2.5 ~ 3m along the Inner Harbour coast, 2 ~ 2.5m on the east of the harbour, and 1 ~ 1.5m along the east coast of the Peninsula. In addition, the coast of Taipa and Coloane also experiences various degree of flood impacts, which are not affected by the storm-tide-alone scenario or tsunami-alone scenario simulations.

The inundation duration for the concurrent storm-tide-tsunami simulation is displayed in Figure 19(d). It shows that the flood on the east coast of Macau Peninsula, two artificial islands, and the coast of Taipa and Coloane, retreats within 1 hour. However, the Inner Harbour area will be submerged in flood water for 2.5 ~ 3 hours. Thus, the coastal area along the Inner Harbour shoreline experiences both maximum inundation depth and the longest inundation duration during the concurrent storm-tide-tsunami scenario.

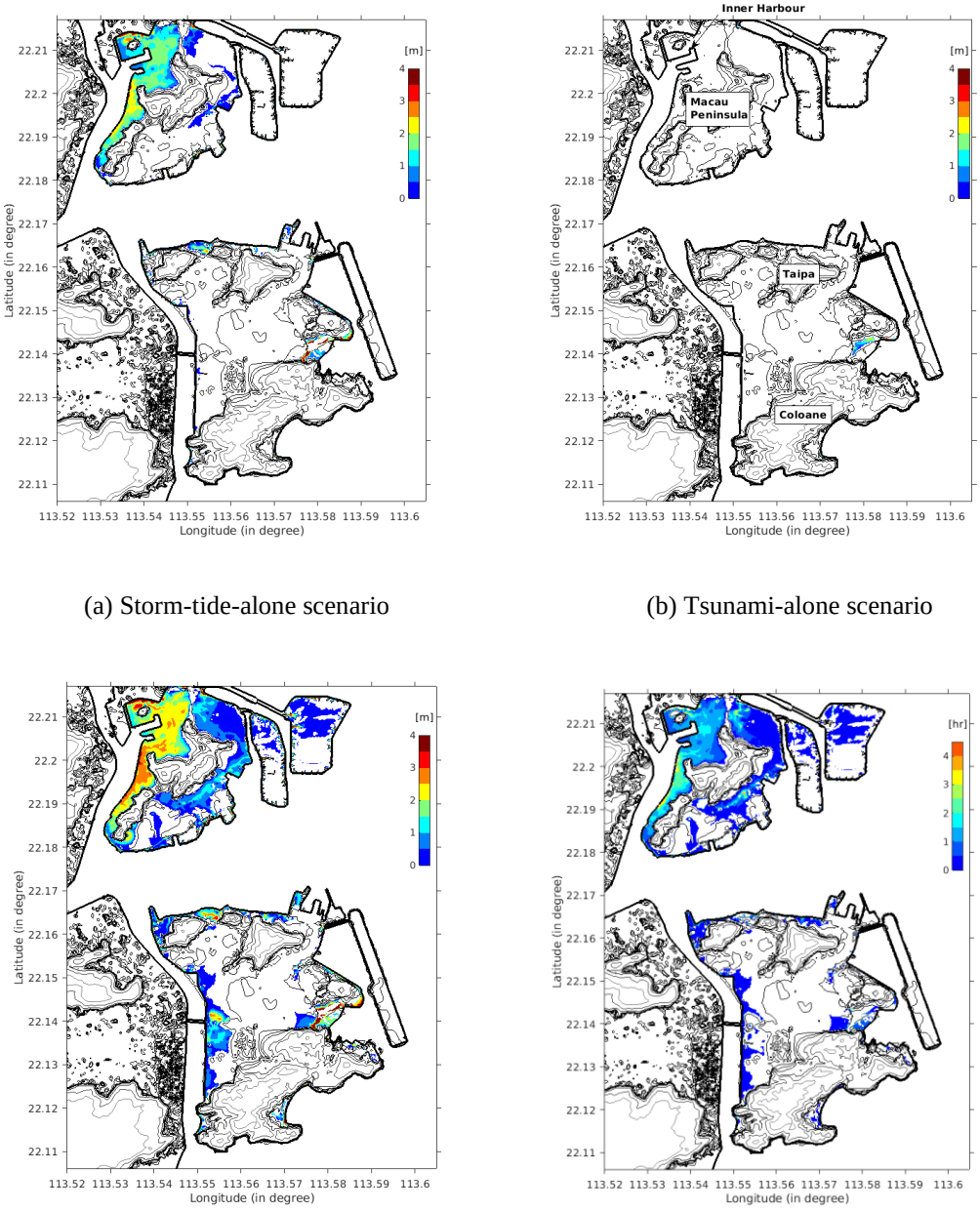

(a) Storm-tide-alone scenario

(b) Tsunami-alone scenario

(c) Concurrent storm-tide-tsunami scenario

(d) Inundation duration for Panel (c) scenario

Figure 19. Maximum inundation water depth and duration at Macau. Panels (a) and (b) show the results for storm-tide-alone scenario and tsunami-alone scenario, respectively. Panel (c) is for the concurrent storm-tide-tsunami scenario. Colour indicates the inundation water depth in metre. Panel (d) shows the flood duration corresponding to (c), and the colour indicates the time in hour.

The inundation patterns of different scenarios in the Kai Tak terminal area in Hong Kong are displayed in Figure 20, in which the panel (a) shows that the storm-tide scenario does not cause any inundation in this area. However, according to the official report (HKO, 2017), the storm surge induced by Typhoon Hato flooded several low-lying areas to the east of Lei Yue Mun, which has not been captured by the present numerical simulation results. The discrepancy may be caused by the uncertainties in bathymetry and topography data due to the rapid urban development, including land reclamation and channel dredging, in this region, which have not always been accurately recorded in the data. Meanwhile, the tsunami-alone scenario floods a few places; Kai Tak terminal is under 1m flood water as shown in

Figure 20(b). In contrast to the storm-tide-alone scenario or tsunami-alone scenario, the concurrent storm-tide-tsunami scenario can cause significant flooding in this region as depicted in Figure 20(c). Both the south and north coasts of the channel are affected, and inundation depth of 1.5 ~ 2m is observed in the vicinity of the terminal and the east of Lei Yue Mun, and 0.5 ~ 1m near Victoria Harbour. Moreover, the flood retreats within 0.4 ~ 0.5 hour in this region as indicated in Figure 20(d).

It should be point out again that all the results presented so far correspond to the scenario where the tsunami is triggered at 7:00 on 23-August-2017, which creates the worst inundation in Macau, but not in the Hong Kong area. To create the worst inundation in the Hong Kong region, tsunamis need to be initiated at 08:10 on 23-Aug-2017. The results of the inundation depth and duration for this worst-case scenario are displayed in Figures 20(e) and (f), respectively. The water depth of 2 ~ 2.5m is observed near the Kai Tak terminal, 1.5 ~ 2m to the east of Lei Yue Mun, and 1 ~ 1.5m near Victoria Harbour. The duration of the worst flood decreases slightly on the east of Lei Yue Mun but increases near the Kai Tak terminal and Victoria Harbour as compared with those shown in Figure 20(d). The flood duration in Hong Kong region is shorter than that in Macau. The reason is that the inundation process in this region is dominated by the tsunamis, hence the flood exhibits a time scale of tsunami wave characteristic period. On the other hand, in Macau the flood is dominated by the storm-tide, which has a longer time scale than tsunami.

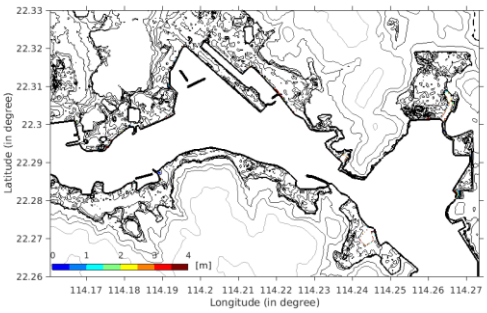

(a) Storm-tide-alone scenario

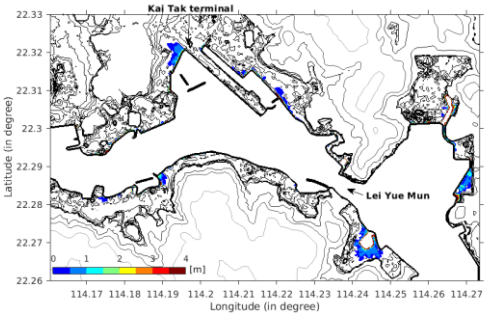

(b) Tsunami-alone scenario

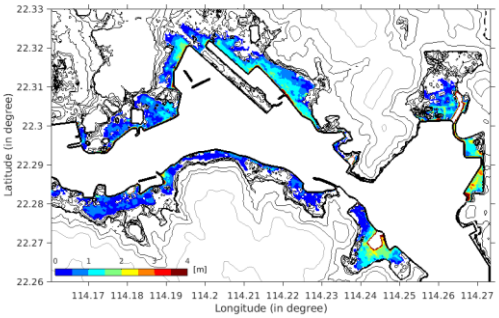

(c) Concurrent storm-tide-tsunami senario

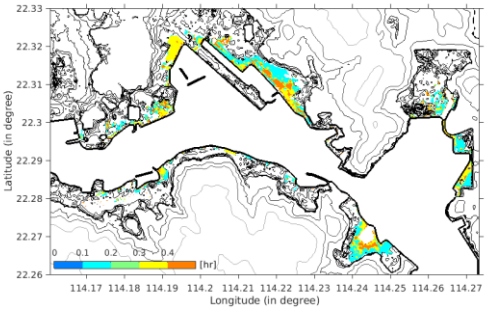

(d) Inundation duration for Panel (c) scenario

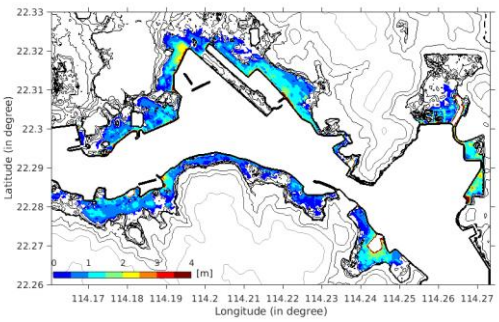

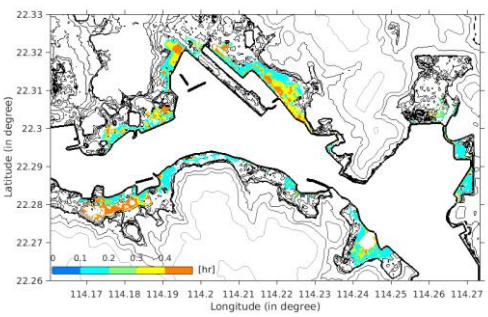

(e) Inundation for concurrent storm-tide-tsunami simulation for the worst-case scenario in HK

(f) Duration for concurrent storm-tide-tsunami simulation for the worst-case scenario in HK

Figure 20. Maximum inundation depth in the vicinity of Kai Tak terminal in Hong Kong. Panels (a) and (b) are the maximum inundation depth corresponding to the storm-tide-alone and tsunami-alone scenarios, respectively. Panel (c) is for the concurrent storm-tide-tsunami scenario. Colour indicates the water depth in metre. Panel (d) is for the flood duration corresponding to the scenario in (c), and the colour indicates the time in hour. Panels (e) and (f) are for worst inundation case in Hong Kong with tsunami initiation time at 08:10 on 23-Aug-2017.

Finally, to demonstrate the importance of the tsunami initiation timing on influencing the extent of inundated area in Macau and Kai Tak terminal region in Hong Kong, the total flooded area (area above MSL and submerged by flood) for the concurrent storm-tide-tsunami events based on the FM results is calculated. The Kai Tak terminal region in Hong Kong is defined as the area within longitude 114.16ºE~114.27ºE and latitude 22.26ºN~22.33ºN (identical to the borders in Figure 20). The inundation areas for different tsunami initiation time are presented in Figure 21. The flooded area in Macau is about 5.3km^2 associated with the storm-tide-alone scenario and 0.7km^2 with the tsunami-alone scenario. However, the concurrent storm-tide-tsunami scenario can inundate 12.0km^2 area when a tsunami is triggered at 07:00 on 23-Aug-2017. This is more than twice the size of the area due to storm-tide-alone, and 16.9 times the area due to tsunami-alone. On the other hand, only 0.6km^2 is flooded in the adjacent Kai Tak terminal region for the storm-tide-alone scenario, and 1.9km^2 area for the tsunami-alone scenario. As mentioned before, the worst-case scenario for flooding in Macau does not coincide with that in Kai Tak terminal region in Hong Kong. Instead, the worst-case scenario for flooding in Kai Tak terminal region is when the tsunami is initiated at 08:10 on 23-Aug-2017 leading to 8.9 km^2 flooded area. The second worst-case scenario correspond to the tsunami initiation time at 06:40 on the same day, yielding a slightly smaller area of 8.8 km^2. In summary, the area of the worst-case scenario for flooding in Kai Tak terminal region is approximately 14.8 and 4.7 times larger than that for the storm-tide-alone scenario and the tsunami-alone scenario, respectively.

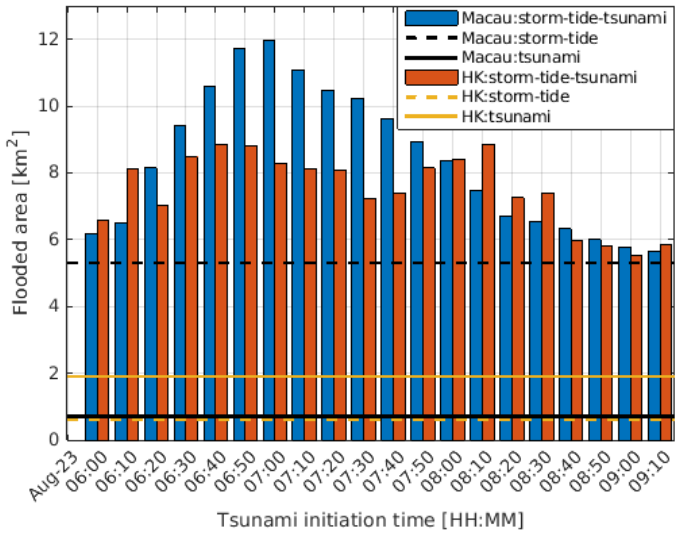

Figure 21. Inundation area against different tsunami initiation time.

5 Concluding remarks

This study investigates the compound impacts of storm-tide and tsunamis on Macau and Hong Kong. The tsunami scenarios are generated by a M_w 9 earthquake in the Manila subduction zone at different hours during a typhoon that resembles to the 2017 Typhoon Hato. The two-way coupled SCHISM-WWMIII model is employed to simulate these synthetic events. The validation results for storm-tide-alone and tsunami-alone simulations indicate that this model can reasonably reproduce these events, separately. For the scenarios simulated, Macau is more affected by the storm-tide, while Hong Kong by the tsunami. A procedure to trigger a tsunami event during an on-going typhoon event is introduced. To study the concurrent storm-tide and tsunami scenarios, using the typhoon Hato condition as the background, 20 scenarios with the tsunami initiation time, varying between 06:00 and 09:10 on 23-Aug-2017, are simulated (the typhoon made landfall at 12:50 on the same day).

The results show that the water level, flow velocity and inundation area in Macau and Hong Kong during the concurrent storm-tide-tsunami event are much higher than those induced by the storm-tide-alone event and the tsunami-alone event. For tsunamis triggered at 7:00 on 23-Aug-2017, resulting in the worst inundation scenario in Macau, the water levels above MSL can reach 4.5 ~ 5m and the flow velocity can be enhanced to 3 ~ 3.5m/s near Inner Harbour in Macau. The Inner Harbour shoreline experiences both maximum inundation depth (2.5 ~ 3m) and the longest inundation duration (2.5 ~ 3 hours) during the concurrent storm-tide-tsunami event. The total inundation area reaches 12.0km^2, which is 2.3 and 16.9 times of the flooding area due to storm-tide-alone and tsunami-alone, respectively. On the other hand, the water level of about 4 ~ 5m and the flow velocity of about 5.5 ~ 6m/s are observed near Kowloon Bay in Hong Kong. It is also noticed that in contrast to Macau, the appearance of vortices is observed near Kowloon Bay. However, they are not found in the storm-tide-alone or tsunami-alone events. In addition, the scenario with tsunamis being initiated at 08:10 on 23-Aug-2017 generates the worst inundation in the Kai Tak terminal region (longitude 114.16^{o}E ~ 114.27^{o}E and latitude 22.26^{o}N ~ 22^{o}N). The inundation depth of 2 ~ 2.5m and duration of 0.4 ~ 0.5 hour are observed in the vicinity of the terminal. The concurrent event floods 8.9 km^2 area in this region, which is 14.8 and 4.7 times of that in the storm-tide-alone scenario and the tsunami-alone scenario.

Furthermore, we compared the results obtained by using the Composite Model (CM) and the Full Model (FM). The former employs the linear superposition of results for two separate simulations, and the latter dynamically models the concurrent event in one simulation. It is found that the CM generally underpredicts the maximum water elevation in the Pearl River estuary for more than 1m, and also reports delayed peak arrival time of more than 10 min. The tidal gauge results show that the maximum water levels predicted by the FM can be 0.88~1.17 times of those by the CM, and the arrival time of the peak flood stage predicted by the FM is 0.87~1.18 times of the CM results. The large spatial and temporal variation of the results between the CM and FM indicates that the FM should be employed for predicting the water levels for a concurrent storm-tide-tsunami event.

In summary, this study provides a numerical tool to simulate the dynamically coupled process that can take place in a concurrent storm-tide-tsunami event. Our results show that the concurrent event can have disastrous consequences in the PRD region. This study can inspire similar research on other regions that are vulnerable to both typhoon/hurricane and tsunami hazards. Nevertheless, the limitation of this study is that the effects of precipitation and watershed drainage were not considered in the current modelling suite. Future work needs to consider meteorological and hydrologic processes more comprehensively. In addition, the conclusions do not hold if the geography, wind or earthquake conditions are changed in the future scenarios.

Acknowledgements

The authors show gratitude to Prof. Kai Meng Mok at University of Macau for providing the navigational charts in the Pearl River estuary and the topographic data of Macau. The numerical model used the topo-bathymetry information obtained from nautical charts of Hong Kong (available at the official site of the Hydrographic Office of the Marine Department of Hong Kong, http://www.hydro.gov.hk), Lidar data of the Civil Engineering and Development Department of Hong Kong (requested at http://www.hyd.gov.hk). The GEBCO 30 arc sec bathymetry data set is freely available at General Bathymetric Chart of the Oceans (http://www.gebco.net/). FES2014 data as the tidal boundary condition in the present model is available at AVISO website for free (http://www.aviso.altimetry.fr/en/home.html). The hindcast products of WAVEWATCH III as the wave boundary condition in the present model are downloaded from IFREMER FTP server (ftp://ftp.ifremer.fr/ifremer/ww3/HINDCAST). The authors also want to thank Dr. Ignacio Sepúlveda for providing the tsunami wave data as the initial condition of the simulations in this study, as well as the COMCOT simulation results. The authors acknowledge the support of a research grant from National Research Foundation to the National University of Singapore (Award number:NRF2018NRF-NSFC003ES-002).

References

Bernard, E. N. & Robinson, A. R., 2009. *Tsunamis*. London, England: Harvard University Press.

Carrere, L., Lyard, F., Cancet, M. & Guillot, A., 2015. *FES 2014, a new tidal model on the global ocean with enhanced accuracy in shallow seas and in the Arctic region.* Vienna, Austria, European Geosciences Union General Assembly.

Chen, J., Wang, Z., Tam, C. Y., Lau, N. C., Lau, D. S. D. & Mok, H. Y., 2020. Impacts of climate change on tropical cyclones and induced storm surges in the Pearl River Delta region using pseudo-global-warming method. *Scientific reports,* 10(1), pp. 1-10.

Chen, Y., Chen, L., Zhang, H. & Gong, W., 2019. Effects of wave-current interaction on the Pearl River Estuary during Typhoon Hato. *Estuarine, Coastal and Shelf Science,* Volume 228, pp. 106364.

Emanuel, K. & Rotunno, R., 2011. Self-stratification of tropical cyclone outflow. Part I: Implications for storm structure. *Journal of the Atmospheric Sciences*, 68(10), pp. 2236-2249.

Gong, W. & Shen, J., 2011. The response of salt intrusion to changes in river discharge and tidal mixing during the dry season in the Modaomen Estuary, China. *Continental Shelf Research,* 31(7-8), pp. 769-788.

HKO, 2017. *Hong Kong Observatory: Super Typhoon Hato (1713) 20 to 24 August 2017.* [Online] Available at: https://www.hko.gov.hk/en/informtc/hato17/report.htm [Accessed 14 06 2021].

Holland, G. J., 1980. An analytic model of the wind and pressure profiles in hurricanes. *Monthly weather review*, 108(8), pp. 1212-1218.

Hsiao, S. C., Wu, H. L., Chen, W. B., Chang, C. H. & Lin, L. Y., 2020. Numerical simulation of large wave heights from super typhoon nepartak (2016) in the eastern waters of Taiwan. *Journal of Marine Science and Engineering,* 8(3), pp. 217.

Hsiao, S. C., Chen, H., Wu, H.L., Chen, W.B., Chang, C.H., Guo, W.D., Chen, Y.M. & Lin, L.Y., 2020. On the Sensitivity of Typhoon Wave Simulations to Tidal Elevation and Current. *Journal of Marine Science and Engineering,* 8(9), pp. 731.

Kowalik, Z. & Proshutinsky, A., 2010. Tsunami–tide interactions: A Cook Inlet case study. *Continental shelf research,* 30(6), pp. 633-642.

Li, L., Switzer, A. D., Chan, C. H., Wang, Y., Weiss, R. & Qiu, Q., 2016. How heterogeneous coseismic slip affects regional probabilistic tsunami hazard assessment: A case study in the South China Sea. *Journal of Geophysical Research: Solid Earth,* 121(8), pp. 6250-6272.

Li, L., Yang, J., Lin, C.Y., Chua, C.T., Wang, Y., Zhao, K., Wu, Y.T., Liu, P.L.-F., Switzer, A.D., Mok, K.M. & Wang, P., 2018. Field survey of Typhoon Hato (2017) and a comparison with storm surge modeling in Macau. *Natural Hazards and Earth System Sciences,* 18(12), pp. 3167–3178.

Liu, P. L.-F., Wang, X. & Salisbury, A. J., 2009. Tsunami hazard and early warning system in South China Sea. *Journal of Asian Earth Sciences,* 36(1), pp. 2–12.

Martínez-Gomariz, E., Gómez, M. & Russo, B., 2016. Experimental study of the stability of pedestrians exposed to urban pluvial flooding. *Natural hazards,* 82(2), pp. 1259-1278.

Megawati, K., Shaw, F., Sieh, K., Huang, Z., Wu, T.R., Lin, Y., Tan, S.K. & Pan, T.C., 2009. Tsunami hazard from the subduction megathrust of the South China Sea: Part I. Source characterization and the resulting tsunami. *Journal of Asian Earth Sciences,* 36(1), pp. 13–20.

Okada, Y., 1985. Surface deformation due to shear and tensile faults in a half-space. *Bulletin of the Seismological Society of America,* 75(4), pp. 1135–1154.

Okal, E. A. & Synolakis, C. E., 2016. Sequencing of tsunami waves: why the first wave is not always the largest. *Geophysical Journal International,* 204(2), pp. 719-735.

Okal, E. A., Synolakis, C. E. & Kalligeris, N., 2011. Tsunami simulations for regional sources in the South China and adjoining seas. *Pure and Applied Geophysics,* 168(6-7), pp. 1153–1173.

Pun, I., Chan, J.C., Lin, I.I., Chan, K.T., Price, J.F., Ko, D.S., Lien, C.C., Wu, Y.L. & Huang, H.C., 2019. Rapid intensification of Typhoon Hato (2017) over shallow water. *Sustainability,* 11(13), pp. 3709.

Roland, A., 2008. *Development of WWM II: Spectral wave modelling on unstructured meshes (Doctoral dissertation).* Darmstadt, Germany:Technische Universität Darmstadt, Institute of Hydraulic and Water Resources Engineering.

Roland, A., Cucco, A., Ferrarin, C., Hsu, T.W., Liau, J.M., Ou, S.H., Umgiesser, G. & Zanke, U., 2009. On the development and verification of a 2-D coupled wave-current model on unstructured meshes. *Journal of Marine Systems,* Volume 78, pp. S244-S254.

Sepúlveda, I., 2017. *Tsunami Hazard Assessments with Consideration of Uncertain Inputs (Doctoral dissertation).* Ithaca, NY, USA: Cornell University.

Sepúlveda, I., Liu, P. L.-F. & Grigoriu, M., 2019. Probabilistic tsunami hazard assessment in South China Sea with consideration of uncertain earthquake characteristics. *Journal of Geophysical Research: Solid Earth,* 124(1), pp. 658-688.

Sepúlveda, I., Liu, P. L.-F., Grigoriu, M. & Pritchard, M., 2017. Tsunami hazard assessments with consideration of uncertain earthquake slip distribution and location. *Journal of Geophysical Research: Solid Earth,* 122(9), pp. 7252-7271.

Shih, H., Chen, H., Liang, T.Y., Fu, H.S., Chang, C.H., Chen, W.B., Su, W.R. & Lin, L.Y., 2018. Generating potential risk maps for typhoon-induced waves along the coast of Taiwan. *Ocean Engineering,* Volume 163, pp. 1-14..

SMG, 2017. *Typhoon Hato <1713>*. [Online] Available at: https://cms.smg.gov.mo/uploads/sync/pdf/tc/2017/c_1713.pdf [Accessed 14 06 2021].

Takagi, H., Yi, X., & Furukawa, F., 2018. Track analysis and storm surge investigation of 2017 Typhoon Hato: were the warning signals issued in Macau and Hong Kong timed appropriately? *Georisk: Assessment and Management of Risk for Engineered Systems and Geohazards,* 12(4), pp. 297-307.

Terry, J. P., Winspear, N., Goff, J. & Tan, P. H., 2017. Past and potential tsunami sources in the South China Sea: A brief synthesis. *Earth-Science Reviews,* Volume 167, pp. 47–61.

Winckler, P., Sepúlveda, I., Aron, F. & Contreras-López, M., 2017. How do tides and tsunamis interact in a highly energetic channel? The case of canal Chacao, Chile. *Journal of Geophysical Research: Oceans,* 122(12), pp. 9605-9624.

Yang, J., Li, L., Zhao, K., Wang, P., Wang, D., Sou, I.M., Yang, Z., Hu, J., Tang, X., Mok, K.M. & Liu, P. L.-F., 2019. A Comparative Study of Typhoon Hato (2017) and Typhoon Mangkhut (2018)—Their Impacts on Coastal Inundation in Macau. *Journal of Geophysical Research: Oceans,* 124(12), pp. 9590-9619.

Yang, J., Lin, C.Y., Liu, H., Li, L., Wu, T.R., Wang, P., Li, B. & Liu, P. L.-F., 2021. Effects of Island Topography on Storm Surge in Taiwan Strait during Typhoon Maria. *Journal of Waterway, Port, Coastal, and Ocean Engineering,* 147(2), pp. 04020057.

Zhang, J., Zheng, J., Jeng, D. S. & Guo, Y., 2015. Numerical simulation of solitary-wave propagation over a steady current. *Journal of Waterway, Port, Coastal, and Ocean Engineering,* 141(3), pp. 04014041.

Zhang, Y. & Baptista, A. M., 2008. SELFE: a semi-implicit Eulerian–Lagrangian finite-element model for cross-scale ocean circulation. *Ocean modelling,* 21(3-4), pp. 71-96.

Zhang, Y. J. & Baptista, A. M., 2008. An efficient and robust tsunami model on unstructured grids. Part I: Inundation benchmarks. *Pure and Applied Geophysics,* 165(11-12), pp. 2229-2248.

Zhang, Y. J., Witter, R. C. & Priest, G. R., 2011. Tsunami–tide interaction in 1964 Prince William Sound tsunami. *Ocean Modelling,* 40(3-4), pp. 246-259.

Zhang, Y. J., Ye, F., Stanev, E. V. & Grashorn, S., 2016. Seamless cross-scale modeling with SCHISM. *Ocean Modelling,* Volume 102, pp. 64-81.